POLITECNICO DI TORINO

Corso di Laurea in Electrical Engineering

Tesi di Laurea Magistrale

Fault tolerant control of modular multilevel shipboard storage system

Relatori
Prof. Michele Angelo Pastorelli
Dr. Fabio Mandrile

Candidato
Umberto Placente

Marzo 2024

Contents

List of Tables

List of Figures

Introduction

In the current context of the maritime industry, electrification is emerging as a key solution to address emissions challenges and improve energy efficiency. The International Maritime Organization (IMO) has set the ambitious goal of reducing greenhouse gas emissions from maritime transport by 50% by 2050 compared to 2008, driving the industry towards the adoption of more sustainable technologies. A crucial element in this transformation is represented by Shipboard Power Systems (SPSs), which are undergoing significant evolution to adapt to the needs of more ecological and efficient navigation. In particular, attention is increasingly focused on Direct Current Shipboard Microgrids (DC-SMGs), which offer numerous advantages over traditional Alternating Current (AC) networks. The introduction of Direct Current (DC) distribution systems has paved the way for a series of innovations, enabling simpler connection of power components and reducing fuel consumption through the use of variable-speed generators and more efficient power flow management. However, along with the benefits, the adoption of DC-SMGs also presents new challenges, particularly regarding the design of protection and fault management systems. Due to their independence from main grids and the harsh operating conditions at sea, shipboard power systems are susceptible to faults and interruptions that can compromise crew safety and equipment onboard. In this context, research on fault-tolerant control plays a crucial role. The aim is to develop strategies and systems capable of efficiently managing faults while ensuring power continuity and system safety.

This thesis aims to address this challenge by focusing on fault-tolerant control of a multilevel modular storage system onboard ships. Through in-depth analysis of system characteristics and the implementation of innovative strategies, the goal is to develop a robust and reliable system capable of ensuring safe and efficient operation even in the presence of faults and unexpected interruptions. Subsequent sections of this thesis will analyze the architecture of SMGs, the types of faults occurring in modules, and the various approaches to fault control adopted, along with the practical implementation of such strategies. Additionally, simulations results obtained through simulations will be examined. Finally, some possible future research directions will be proposed, aiming to contribute to the development of increasingly safe, efficient, and sustainable maritime power systems.

Chapter 1

Power Configurations for Shipboard DC-SMG Systems

The power requirements on a vessel typically reach megawatt (MW) levels, which low-voltage SPSs are unable to fulfill. Additionally, diverse types of vessels possess distinct power supply needs related to reliability, energy density, flexibility, and other factors. Hence, examining the bus structure, voltage levels, and system setup of SPSs becomes essential.

1.1 Bus Configuration and Voltage Levels

In the realm of DC networks, two distinct DC bus architectures prevail: the unipolar and bipolar bus topologies. In unipolar setups, all components are linked to a two-wire DC bus, comprising positive and negative poles, via converters. While straightforward in design, the unipolar system lacks redundancy and remains vulnerable even to a singular fault occurrence. Conversely, the bipolar configuration employs three wires—positive, negative, and neutral. Compared to its unipolar counterpart, the bipolar system offers

enhanced power capacity, heightened reliability, reduced transmission losses due to lower currents in the return wire, and greater flexibility in load and distributed generation connections. However, the bipolar architecture's ability to accommodate varying voltage levels may lead to load imbalances, necessitating a voltage balancing circuit to stabilize the DC bus voltage. Despite this challenge, the majority of existing DC-SMGs adhere to the bipolar architecture. As of now, no standardized protocol governs the determination of DC voltage levels for DC-SMGs. Determining the system voltage entails factoring in cost considerations, desired generator and propulsion motor drive voltages, converter design, load specifications, cable and bus-bar ratings, and fault energy. In practice, distribution system voltage levels fluctuate based on power requirements and vessel types. Recommended MVdc voltage levels for SMG systems, with a ±10% DC bus voltage tolerance, are depicted in Figure 1.1.

	MVDC Class	Nominal MVDC Class Rated Voltage	Maximum MVDC Class Rated Voltage
Already Established	1.5	1.5 or ±0.75	2 or ±1
	3	3 or ±1.5	5 or ±2.5
Future Design	6	6 or ±3	10 or ±5
	12	12 or ±6	16 or ±8
	18	18 or ±9	22 or ±11
	24	24 or ±12	28 or ±14
	30	30 or ±15	34 or ±17

Figure 1.1: MVDC voltages ranges (kV).
Source: [1]

1.2 General shipboard system

In the context of direct current (DC) vessels, power supply devices generally include the following components: power generation modules (PGMs), energy storage systems (ESS), propulsion systems, and loads.

1.2.1 Power Generation

Generators

Power generation components must ensure efficiency and environmental sustainability. Currently, the primary power sources on ships are diesel generators, while the introduction of fuel cells (FCs) for marine applications is still in development. Marine generators within DC power systems consist of primary engines, generators, and rectifiers. These generators can be of two main types: wound-rotor synchronous machines (WRSM) and permanent-magnet synchronous machines (PMSM). The output of generators, initially in alternating current, is converted to direct current by rectifiers to adapt to Direct Current Power Generation Systems (DC-PGS). In figure 1.2

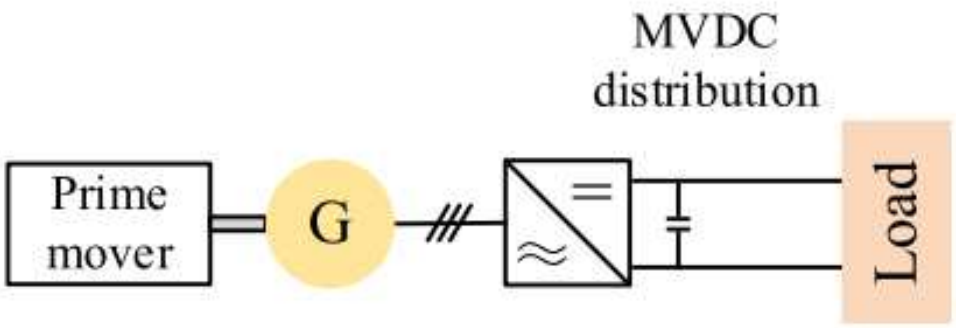

Figure 1.2: Simplified generation module in MVdc distribution.
Source: [1]

Fuel Cells

Fuel cells serve as emission-free power sources. Various types of cells exist, including alkaline fuel cells (AFC), proton exchange membrane fuel cells (PEMFC), direct methanol fuel cells, and solid oxide fuel cells (SOFC), converting chemical energy into electrical energy. The direct current output of fuel cells is regulated through DC/DC converters for effective integration into DC-PGS.

1.2.2 Energy Storage Systems (ESS)

To ensure economical and reliable operation, ESSs are essential in marine vessels. They offer several advantages, including spinning reserve, peak power reduction, and network stability. Moreover, during generator system failures or isolations of non-interruptible parts, ESSs act as backup power sources. The choice of ESS technology depends on various factors such as required power, energy density, and costs. Batteries, integrated into DC-PGS through DC/DC converters, are one of the most common options. However, to overcome challenges associated with centralized battery configurations, the concept of distributed battery energy storage systems is being developed, where each battery cell is equipped with a converter module. Configurations of these systems, both centralized and distributed, are illustrated for clarity in figure 1.3.

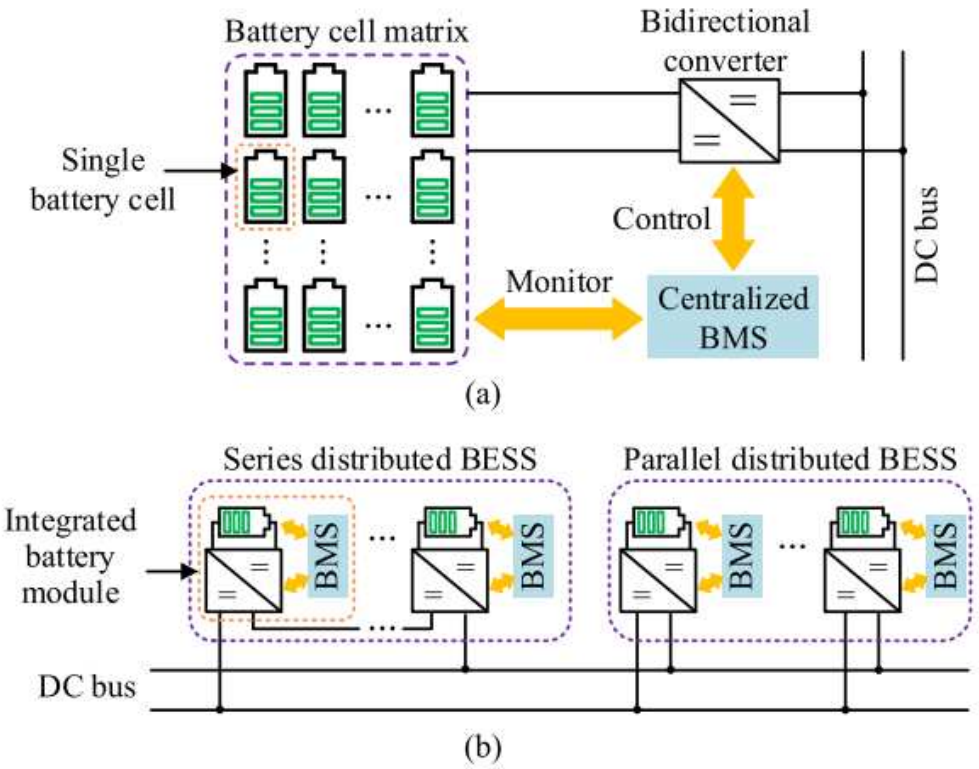

Figure 1.3: Centralized (a) and distributed (a) BESS configuration.
Source: [1]

1.3 Switch faults and module failures

To better contextualize the thesis topic and introduce the proposed solution, it will be helpful to present the schema of the modular multilevel storage system. As shown in figure 1.4, the system comprises several storage units, each equipped with its converter. This modular approach offers numerous advantages, including increased flexibility and system reliability. However, the presence of faults can compromise the proper functioning of the entire system, making the implementation of a fault-tolerant control system crucial.

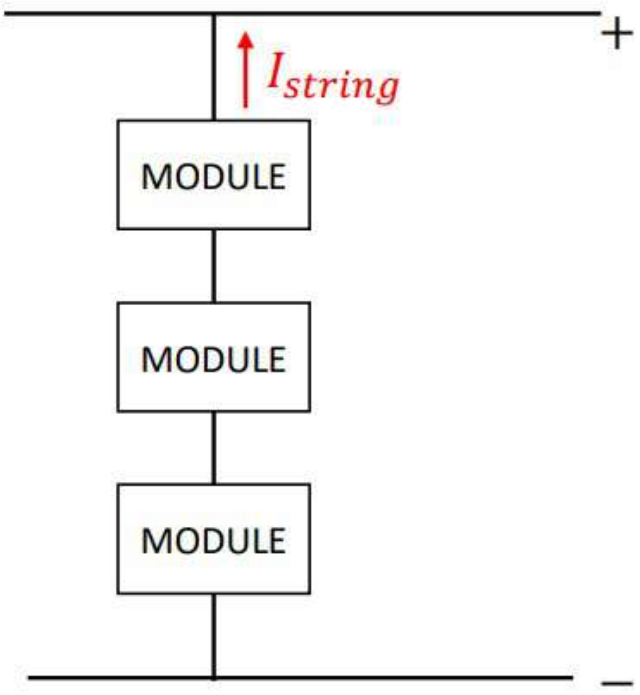

Figure 1.4: Schematic of the modular multilevel storage system.

The primary aim of this thesis is to investigate the consequences of failures in multilevel modular storage systems and propose solutions to ensure continuous system operation with the required performance. To achieve this goal, implementing a fault-tolerant control system is necessary. Before delving into control strategies, it is crucial to understand the causes of failures within modular converters. Failures in modules are mainly caused by open-circuit interruptions or short-circuits in the switches. Short-circuits in the switches are typically triggered by environmental factors such as humidity and temperature variations, or operational factors like overcurrent, overvoltage, and high junction temperature. These faults can lead to significant damage and result in high overcurrent

within a short time frame. The short-circuit faults in the upper and lower switches are shown in figure 1.5, respectively. Identifying these faults promptly is crucial for ensuring the continuous operation of the system.

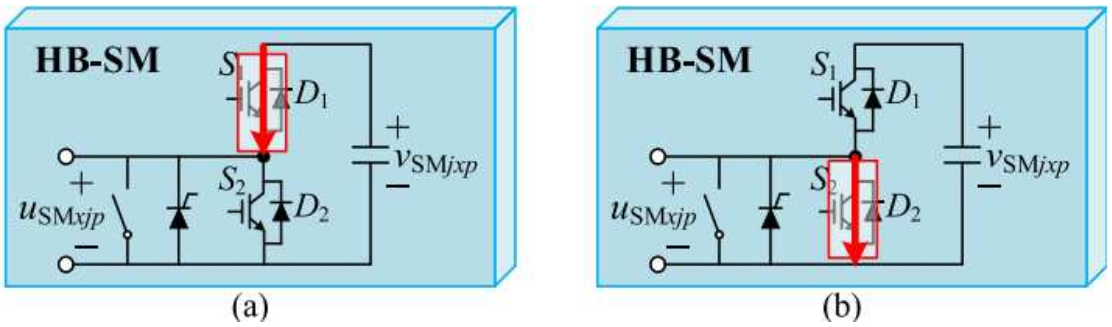

Figure 1.5: Short circuit fault in a singole module.
Source: [2]

On the other hand, open-circuit interruptions in the switches are usually caused by unavailable drive signals, internal wire connection ruptures, bond wire lift-offs, etc. These faults can cause secondary damage to the device if not promptly detected, potentially leading to system failure. The open-circuit faults in the upper and lower switches are demonstrated in figure 1.6 respectively. It's essential to identify and address these faults swiftly to maintain the integrity and reliability of the system.

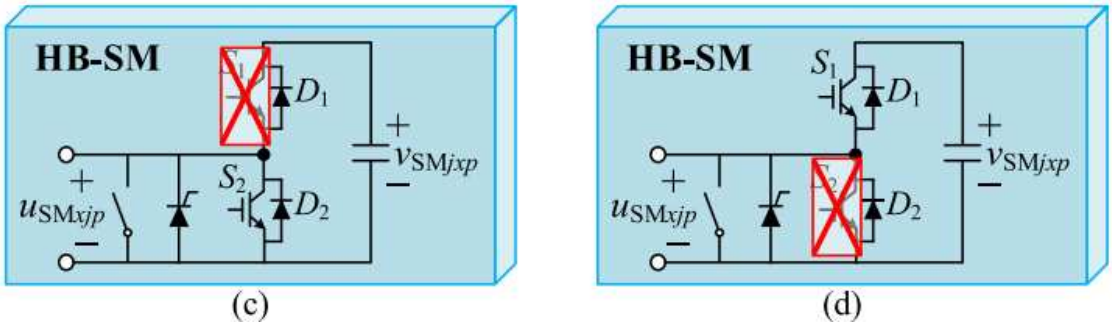

Figure 1.6: Open circuit fault in a singole module.
Source: [2]

To ensure continuous operation of the modular multilevel converter (MMC), faulty

modules need to be promptly identified, and fault-tolerant control is essential before replacing them.

Chapter 2

Configuration and control of modular systems

This chapter will delve into the intricacies of modular multilevel storage systems. Subsequently, it will address the configuration employed for this thesis and the sizing of the battery pack. Towards the conclusion of this chapter, the implemented control strategies for all simulations will be thoroughly discussed.

2.1 Module configuration

Modern energy storage systems typically consist of a battery pack and a converter, which together form a module. Both components are essential for regulating energy input and output. The battery pack may comprise a variable number of cells connected in series or parallel, depending on specific performance and voltage requirements. The converter, commonly designed with two switches and antiparallel diodes, plays a crucial role in regulating the output voltage of the storage system, ensuring efficient and safe energy delivery. Figure 2.1 illustrates a representation of the individual module.

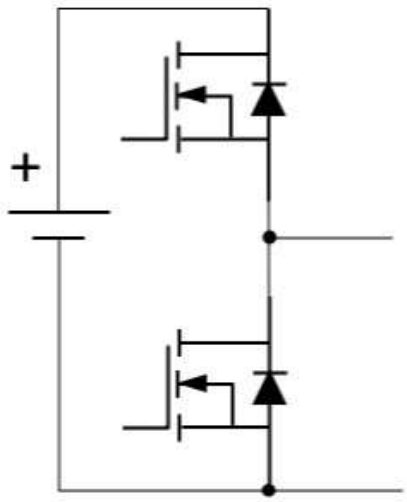

Figure 2.1: Module schematic.

In modular systems, the configuration of modules can significantly influence the overall system performance. There are two main types of output configuration commonly adopted between modules:

- series connection
- parallel connection.

2.1.1 Series connection

Series Connection between Modules involves connecting modules in series, meaning that the output of one module is directly connected to the input of the next. A representation of this configuration is depicted in Figure 2.2.

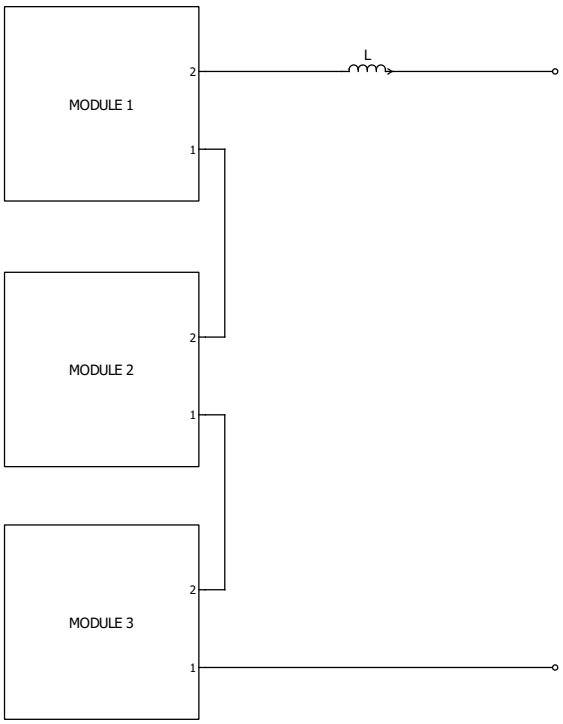

Figure 2.2: Modules in series.

The benefits derived from this configuration are as follows:

- Increase in Output Voltage: Connecting modules in series allows for an increase in the overall output voltage of the system.
- Reduction in Required Current: This configuration enables a reduction in the required current on each individual module.
- Flexibility in System Sizing: Series connection provides greater flexibility in system sizing, allowing for adaptation to specific application requirements.

Conversely, the disadvantages are:

- Sensitivity to Voltage Fluctuations: The system becomes more sensitive to external voltage fluctuations, potentially damaging or compromising component operation.

- Complexity of Voltage Balancing: Special attention is required for voltage balancing among series-connected modules, as variations can decrease system efficiency and lifespan.

- Risk of Cascade Failures: A malfunction in a single module in series can impact the entire system.

These considerations highlight the trade-offs associated with series connection in modular systems.

2.1.2 Parallel connection

In the context of parallel connection between modules, it involves connecting the like poles of the modules. A representation of this configuration is depicted in Figure 2.3.

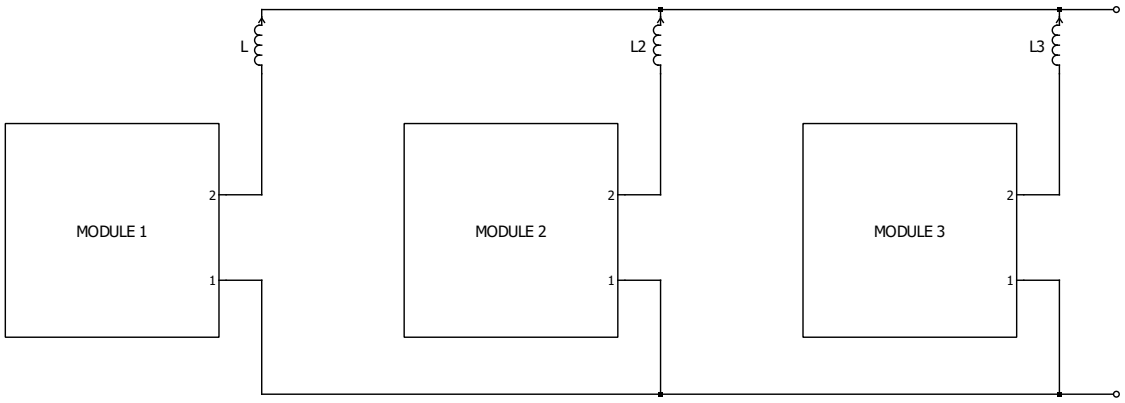

Figure 2.3: Modules in parallel.

The benefits derived from this configuration are as follows:

- Increase in Output Current: This configuration is beneficial for achieving a higher overall output current of the system. It allows for the combination of individual module currents, resulting in a greater total current output.

- Utilization with Large Battery Packs: It is particularly advantageous when working with large battery packs. The parallel connection enables efficient utilization of the capacity of each individual module, thereby enhancing the performance of the system, especially in applications requiring high current output.

- Redundancy Capability: The redundancy capability is a notable advantage of parallel connection. In case of a failure of one module in parallel, it does not impact the entire system. This enhances the reliability and fault tolerance of the overall system.

Conversely, the disadvantages are:

- Current sharing Complexity: It is necessary to evenly balance the current among the modules in parallel to avoid overloads and overheating. This ensures that each module carries its fair share of the load, maintaining system stability and preventing any individual module from being overloaded.

- Decreased efficiency at Low Loads: In some cases, parallel connection may reduce the system efficiency at low loads. This occurs because the combined output of multiple modules in parallel may not scale linearly with the load, resulting in decreased efficiency at lighter loads due to increased losses in the system.

For the implementation of the system's module connection regarding the thesis, the choice was made based on the required output performance and the desire to observe the behavior of a multilevel modular system following a fault within a module. In the subsequent chapters, the circuits used will be presented.

2.2 Sizing of battery pack

The objective of the simulated system is to faithfully replicate the behavior of a scaled-up real-world counterpart, ensuring that the simulations accurately reflect the performance and characteristics of the actual system. In pursuit of this goal, careful selection of system components is paramount. For these simulations, modules operating at 600 V output have been chosen. By connecting these modules in series, they can collectively provide the required voltage of 1000 V at the load. This series connection configuration offers a practical solution to meet the voltage demands of the system's intended application. However, in addition to achieving the desired output voltage, the study undertaken in this thesis also seeks to explore the system's response in the event of a module failure. To comprehensively investigate this scenario, three modules are considered in the simulations. This redundancy ensures that even in the event of a fault occurring in one of the modules, the system can still deliver the required performance, namely the desired 1000 V output voltage. In this context, the selection of an appropriate cell model is crucial for accurately representing the behavior of the battery system in the simulations. Thus, the cylindrical cell model, specifically the Panasonic CGR18650CG, has been chosen for its suitability and relevance to the system under study. Table 2.1 provides an overview of the crucial parameters of the selected cell model, offering insights into its characteristics and performance. Furthermore, the battery model used in the simulation is depicted in Figure 2.4, providing a visual representation of the system's configuration and components. By meticulously selecting the components and configuring the system parameters, the simulated system aims to provide valuable insights into the behavior and performance of the real-world system, contributing to a deeper understanding of its operation and potential responses to various scenarios.

Cell Parameters	
$Brand$	Panasonic
$Model$	CGR18650CG
V_{cell}	3.6 V
$Capacity$	2250 mAh

Table 2.1: Main parameters of Panasonic CGR18650CG

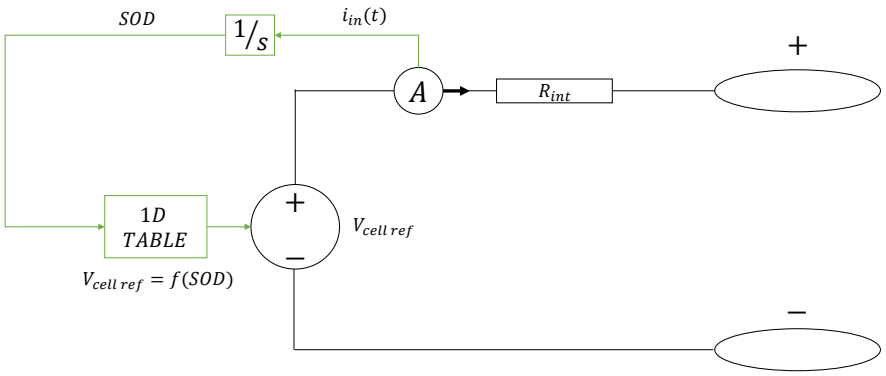

Figure 2.4: Battery model.
Source: [3]

To achieve the desired 600 V voltage, a specific number of cells have been connected in series. In order to minimize simulation times, a certain number of cells have been connected in parallel, but kept below unity. This approach helps in reducing the overall capacity of the battery pack. Below is the calculation determining the required number of cells in series to attain an output voltage from the battery pack equal to 600 V.

$$N_{\text{cell}} = \frac{V_{\text{batt}}}{V_{\text{cell}}} = \frac{600}{3.6} \approx 167\ cells \tag{2.1}$$

Considering this type of model, we can calculate the discharge time of a single battery

pack using the equation 2.2.

$$Time = \frac{Capacity}{Current} \tag{2.2}$$

where:

- $Time$ represents the discharge time (measured in hours if capacity is in mAh and current in mA).
- $Capacity$ denotes the capacity of the cell or battery pack (measured in mAh or Ah).
- $Current$ is the discharge current (measured in mA or A).

Based on the simulations conducted, the number of cells in parallel n_p was varied, but the equation 2.2 was consistently applied to calculate the discharge time.

2.3 Control Implementation

For this simulation, two control loops have been implemented: an internal current control loop and an external voltage control loop. It is crucial to emphasize that for the cascaded control system to operate efficiently, the internal loop must have a higher bandwidth compared to the external loop. The configuration of the internal control loop is depicted in figure 2.5, and below are its sizing details.

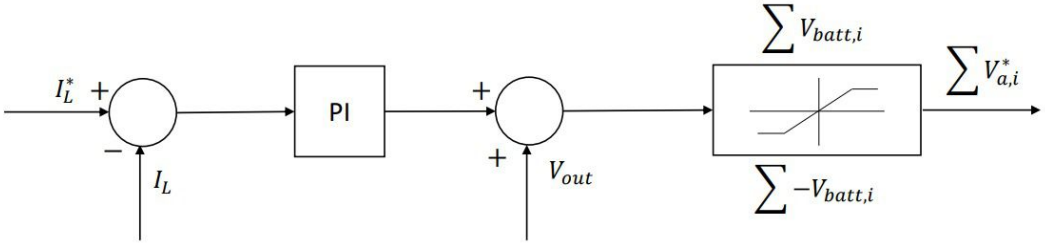

Figure 2.5: Current control

$$\begin{cases} K_{p,I} = \omega_{b,I} \cdot L \\ K_{i,I} \leq 0.1 \cdot K_{p,I} \cdot \omega_{b,I} \end{cases} \tag{2.3}$$

The external voltage loop is illustrated in figure 2.6. Its sizing is determined using the same method applied to the internal current loop.

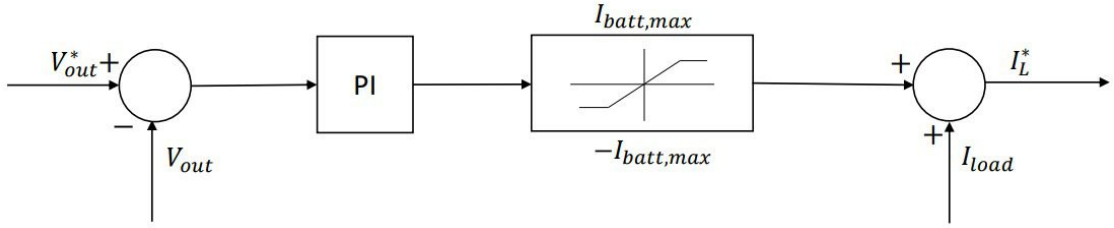

Figure 2.6: Voltage control

$$\begin{cases} K_{p,V} = \omega_{b,V} \cdot C \\ K_{i,V} \leq 0.1 \cdot K_{p,V} \cdot \omega_{b,V} \end{cases} \tag{2.4}$$

Both control loops have been configured with a Proportional-Integral control strategy to nullify steady-state errors. This approach ensures that the system achieves and maintains the desired state without any residual deviation over time.

In the case of charging, voltage control is unnecessary as it is already fixed by an ideal voltage source; hence, only current control will be implemented. To conclude this section, the calculation of duty cycles for each individual module is presented. An example with three modules arranged in series is provided for illustration, as depicted in Figure 2.7.

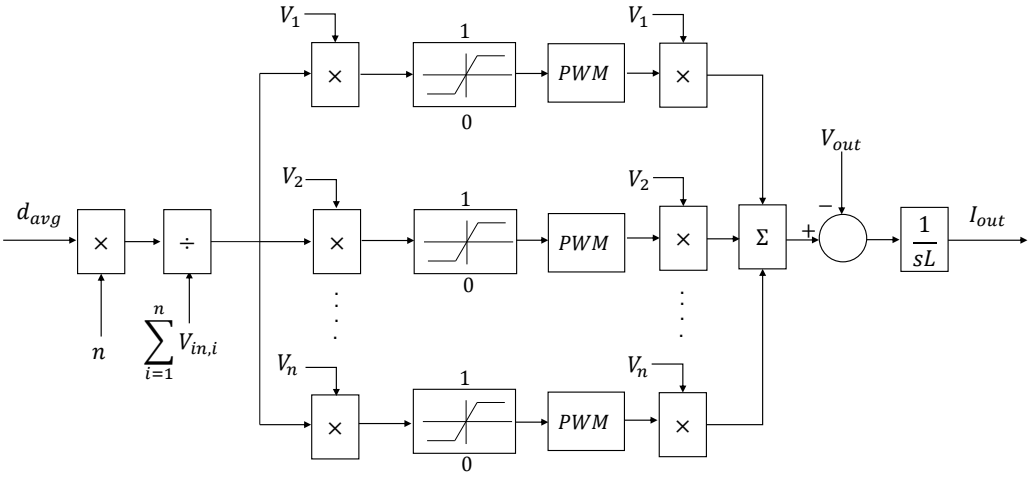

Figure 2.7: Duty cycle calcolation for three modules in series.
Source: [3]

Chapter 3

Fault-tolerant control

This chapter will explore the various fault-tolerant control strategies employed in modular multilevel storage system. Subsequently, it will discuss the controls implemented for the thesis and offer insights into predicting module or string failures.

3.1 Fault-tolerant control strategies

Modular multilevel shipboard storage systems are precisely engineered to meet stringent electrical voltage and current specifications, ensuring seamless operation and requisite performance standards. To fortify these systems against potential disruptions, fault-tolerant control mechanisms are indispensably implemented. Within the literature, a comprehensive classification of fault-tolerant strategies customized for modular multilevel system is available, as depicted in Figure 3.1.

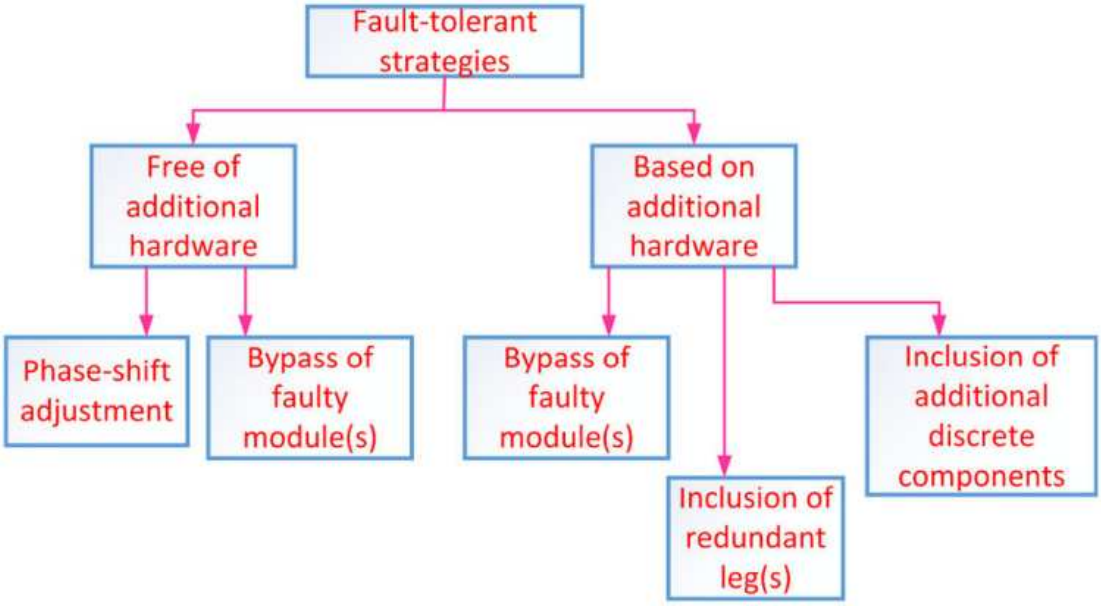

Figure 3.1: Fault-tolerant strategies.
Source:[4]

As illustrated in figure 3.1, fault-tolerant control methods can be divided into two main categories: those without the addition of extra hardware and those with an additional hardware within the system. I will now delve into these categories in more detail.

3.1.1 Phase-shift adjustment

The first method under discussion is Phase-shift adjustment, which involves adjusting gating signals following a module fault. This means modifying the phase shift between control signals to adapt to the active components/switches of the converter. Figure 3.2 depicts the cases without reconfiguration (a) and with phase shift reconfiguration (b).

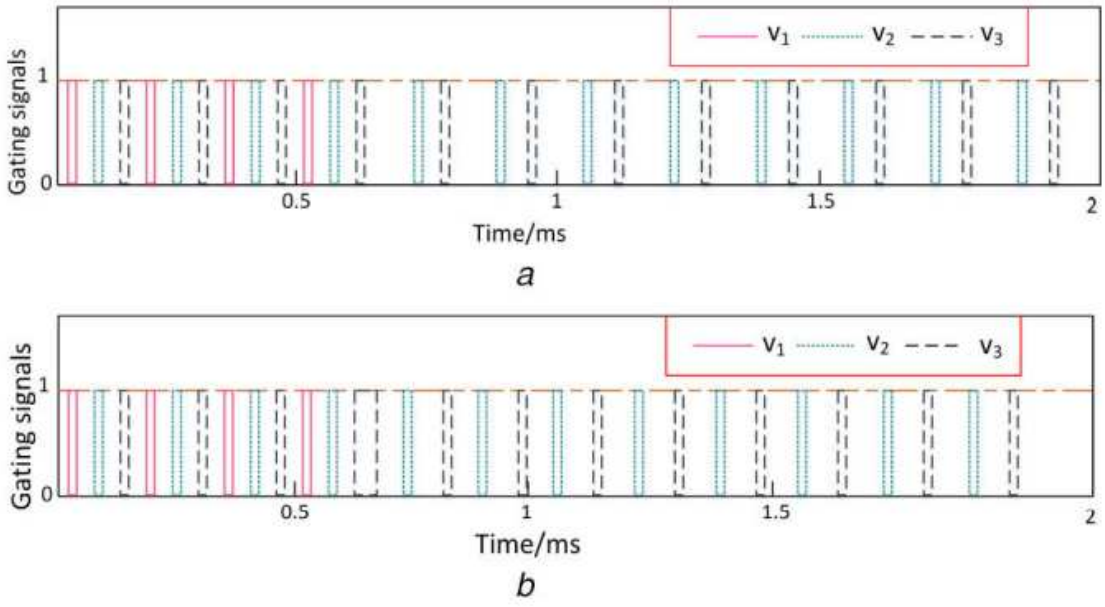

Figure 3.2: Phase-shift adjustment.
Source:[4]

After identifying the fault, the gating signal associated with the faulty switch, which affects the switch controlled by signal q1, is removed from the switching model, leaving only signals q2 and q3. At this point, the phase shift applied between the gating signals is corrected. In figure 3.2, the gating signals q3 and q2 are adjusted by radians after t=0.55 ms. The key benefits of the fault-tolerant strategy through phase shift adjustment are:

- Low implementation cost
- Efficiency and simplicity

This method is usually employed when modules are connected in series, and phase shift is applied to reduce the harmonic content in the output, namely the current ripple. Without a module, the absence of one of the components would compromise the system's

symmetry, leading to distortions in the current waveform and impacting overall harmonic performance.

3.1.2 Bypass of faulty module

Another fault-tolerant control method is the bypass of faulty module, as depicted in figure 3.3.

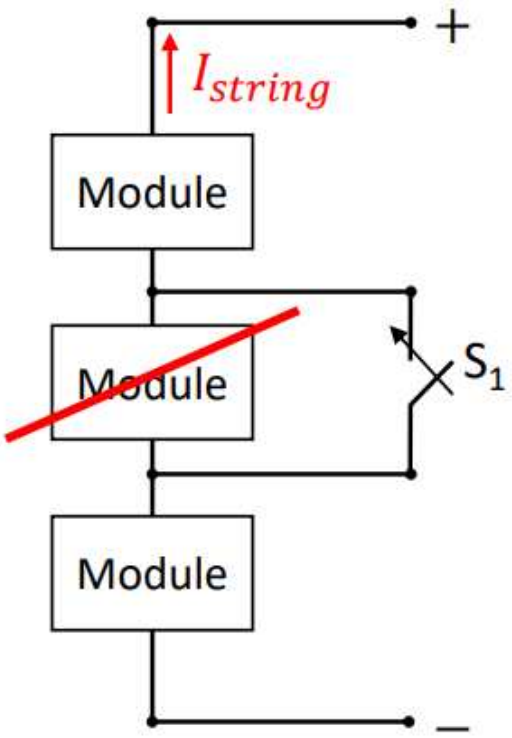

Figure 3.3: Bypass of faulty module.

The system consists of 3 modules that participate during normal conditions. When a fault occurs in one module, the system detects the fault, and the faulty module is bypassed, allowing only the healthy modules to operate. The advantages of through bypass of faulty module are:

- No changes in the original control scheme
- no control reconfiguration

3.1.3 Redundant module with bypass of faulty module

In this scenario, additional components are incorporated into the system. According to the literature, there are primarily two types of redundancies in the MMC:

- Cold-reserve redundancy
- Hot-reserve redundancy

Cold-Reserve/Passive Redundancy-Based Methods

For cold-reserve redundancy-based methods, redundant modules are bypassed during normal conditions. When an SM failure occurs, the redundant modules begin to participate in the operation. This type of control is illustrated in figure 3.4.

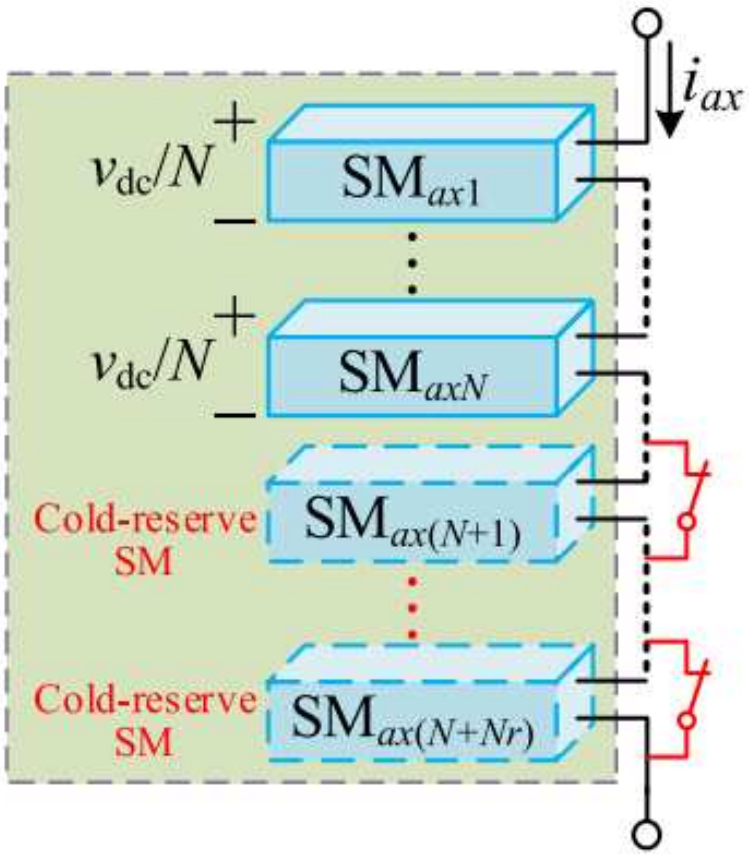

Figure 3.4: Bypass with cold-reserve redundancy- based methods
Source:[2]

Cold-reserve redundancy-based methods typically involve fewer modules and result in lower power loss. However, harmonic performance is limited, and there is higher voltage stress due to the reduced operation of modules.

Hot-Reserve/Passive Redundancy-Based Methods

In hot-reserve redundancy-based methods, redundant modules actively participate during normal operating conditions, with module voltages operating at a lower value. This approach offers several key advantages, including reduced voltage stress on individual modules and lower circulating current. An example of this method is illustrated in Figure

3.5.

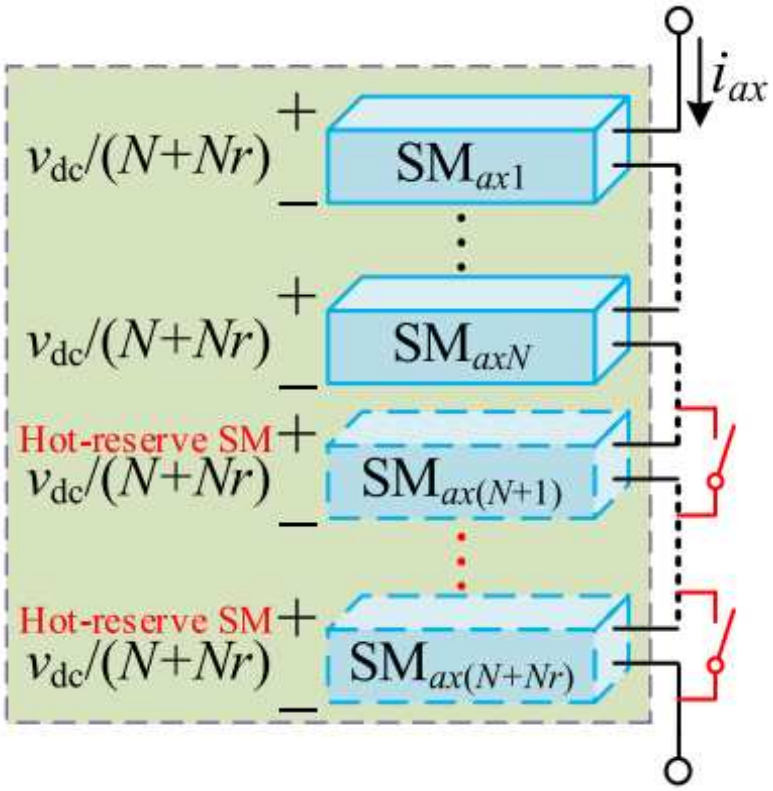

Figure 3.5: Bypass with hot-reserve redundancy- based methods
Source:[2]

When a fault occurs in a module, the output voltages of healthy modules increase to restore the normal output voltage range, while the faulty modules are bypassed. Subsequently, the voltages of the remaining healthy modules are increased to maintain the normal output voltage range of the faulty phase. While hot-reserve redundancy-based methods can mitigate or avoid challenges associated with increased output voltage in comparison to cold-reserve redundancy-based methods, they typically entail higher switching losses with similar harmonic performance.

Integrated Redundancy-Based Methods

In this case, both cold-reserve and hot-reserve control methods are employed. When an SM failure occurs, hot-reserve SMs can ensure seamless fault-tolerant control. Simultaneously, cold-reserve SMs are reconfigured as hot-reserve SMs, allowing seamless fault-tolerant control to be maintained with reduced power losses.

3.1.4 Inclusion of redundant leg(s)

The addition of redundant legs is a fault-tolerant architecture that prevents operational discontinuity in the event of a failure. Typically, redundant legs consist of redundant switches and, when applicable, other auxiliary components. A prime example of redundant leg-based architecture is the fault-tolerant structure of the single-switch DC-DC boost converter. The redundant leg comprises either a single switch or a TRIAC and a switch, associated in parallel with the original converter.

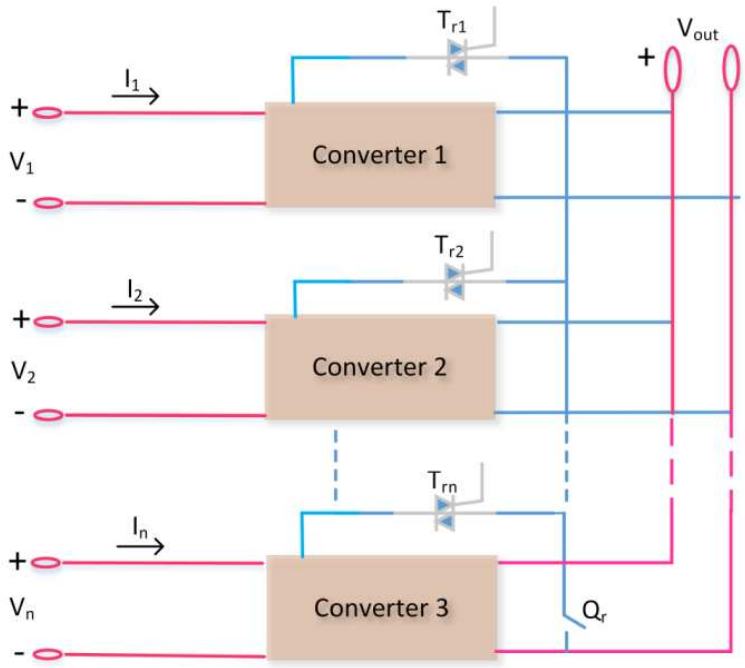

Figure 3.6: Bypass with inclusion of redundant leg(s)
Source: [4]

As illustrated in Figure 3.6, the redundant leg is activated upon a failure in the original converter switch. Implementing this strategy becomes cost-effective and offers an appealing solution, especially when dealing with a number of single-switch DC-DC boost converters.

3.1.5 Inclusion of additional discrete components

This technique employs additional discrete components, distinct from those found in standard DC-DC converters. The additional components in these fault-tolerant devices do not directly interfere with the functions of the faulty switches. This approach is typically used in full-bridge converters as open-circuit switch faults can result in a reduction in output voltage. To counteract this reduction, the reconfiguration strategy plays a crucial role. Such systems, designed to withstand faults, require the addition of an auxiliary

transformer winding, usually placed in the secondary circuit, as illustrated in figure 3.7.

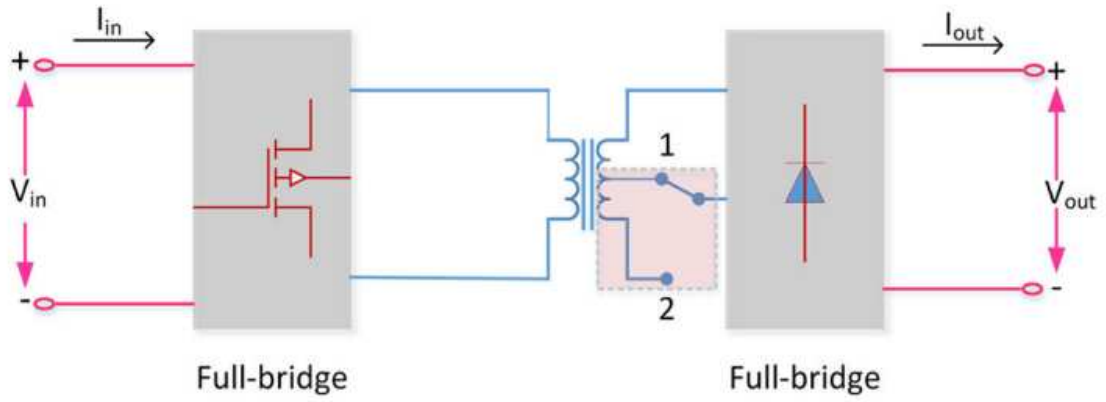

Figure 3.7: Bypass with inclusion of additional discrete components
Source: [4]

If a fault disrupts the operation of the bridge on the transformer's primary side, the auxiliary winding is activated to compensate for the voltage drop. However, integrating this winding incurs significant implementation costs.

3.2 Selected fault-tolerant approaches

Based on the types of fault-tolerant control methods analyzed in the previous section, we have opted to implement two specific approaches:

- phase-shift adjustment
- bypass of faulty module

This decision stems from the fact that, when SM failures occur, the faulty modules cannot be immediately replaced and we want obtain the performance required. Initially, we implemented these methods in ideal scenarios to assess their potential effects. Subsequently, we plan to apply these techniques to some cases studies to evaluate their applicability and effectiveness in practical contexts.

3.2.1 Phase-shift Adjustment implementation

There are various methods to implement this type of control, but the one used in these simulations is chosen due to the assumption that the switches cannot increase their frequency. For the implementation of this control, the following parameters need to be known:

- Switching frequency
- Phase shift angle between the carriers
- Number of faulty modules
- Number of redundant modules

With this information, the phase shift angle between the carriers is adjusted to achieve identical switching harmonic cancellation. In a general case, the phase shift angle should be varied according to:

$$\frac{2 \cdot \pi}{N_a + N_r - N_f} \tag{3.1}$$

Where:

- N_a stands for the number of ordinary modules
- N_r stands for the number of redundant modules
- N_f stands for the number of faulty modules

In simulation contexts, one critical aspect lies in the control of phase shifting. This is achieved through the utilization of a component known as "Variable Phase PWM". This block takes the duty cycle and desired phase as inputs, and outputs the gating signal q.

The desired phase value is set by a digital controller that monitors the state of switches within the converter. Should the switches find themselves in the same state, the system detects a fault within the converter. Consequently, in properly functioning converters, the system automatically adjusts the phase shifting.

The figure 3.8 illustrates the block employed to implement this mechanism.

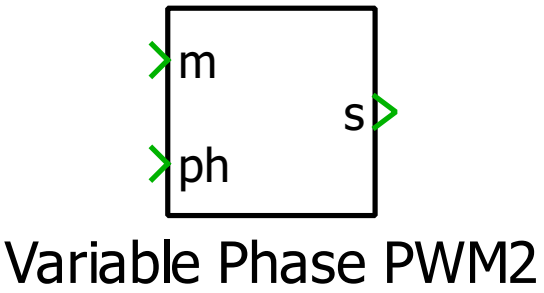

Figure 3.8: Variable phase PWM.

3.2.2 Bypass implementation

Regarding the implementation of the bypass, a specific approach was chosen. Similar to the phase shift implementation, the gating signals of the two switches are monitored. If they are found to be in the same state, indicating a potential fault, the module is bypassed by closing switch S1. The figure below, labeled as "Bypass Implemented" in reference 3.9, visually illustrates the aforementioned process.

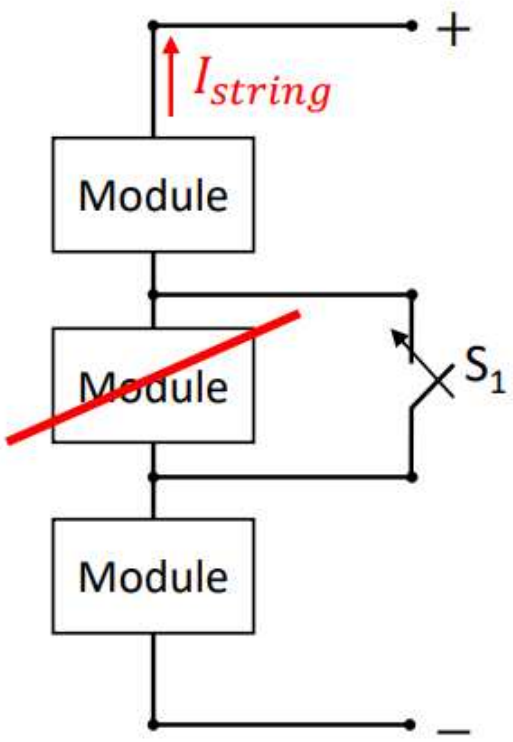

Figure 3.9: Bypass implemented.

3.2.3 Ideal discharge mode

For the initial simulation, we focused on the discharge mode. In this setup, the system comprises three battery packs, each equipped with its own converter. To ensure effective current filtering, an inductor has been integrated. Given the idealized nature of this scenario, the load is represented by an ideal voltage source. The system configuration is depicted in figure 3.10 providing a visual representation of the components involved.

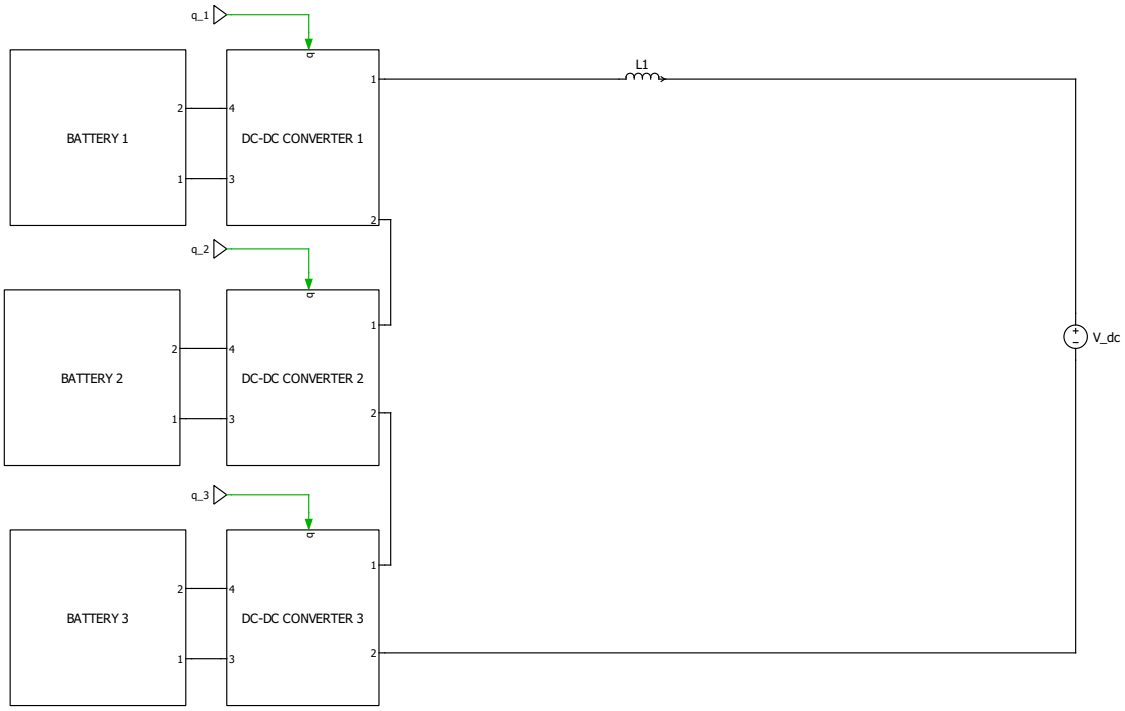

Figure 3.10: Ideal system for discharge mode.

Following a fault occurrence in one of the converters, particularly in the case of an open-circuit fault, the control over the converter's switches is lost. Consequently, the current will circulate through the diode in anti-parallel with the low-side switch, rendering the battery pack unable to supply current, as illustrated in figure 3.11. It's worth noting that the diode in anti-parallel is designed to withstand the reverse current, ensuring continuity of operation in the system.

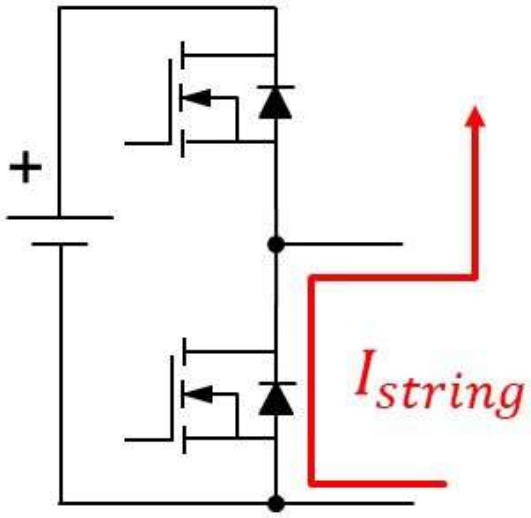

Figure 3.11: Current string.

From a system perspective, service continuity is maintained, even though with a reduction in harmonic performance, as depicted in figure 3.12

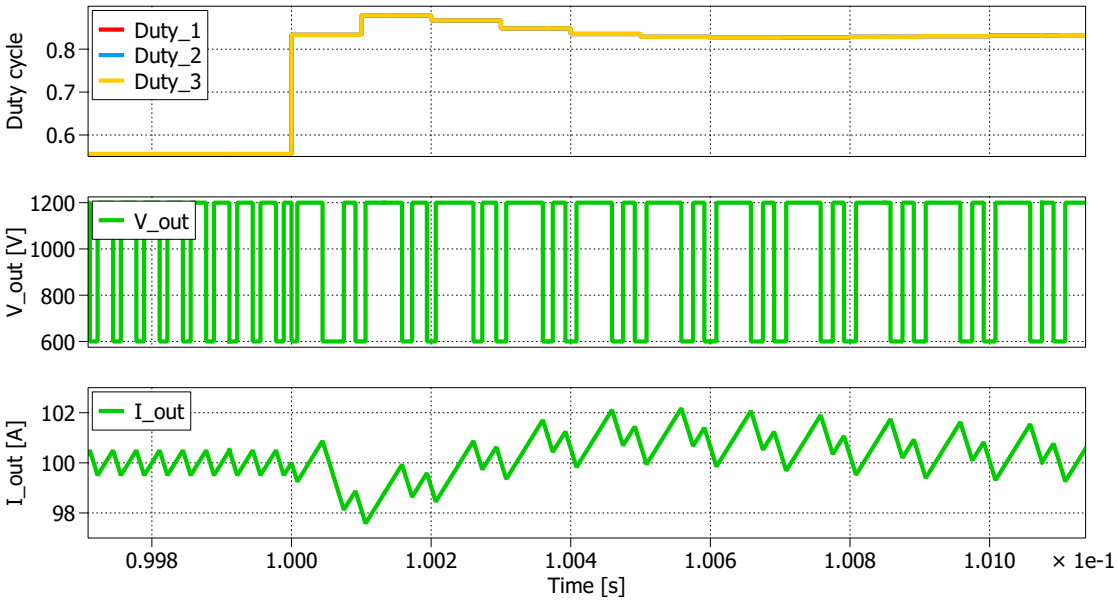

Figure 3.12: Output values without fault tolerant control.

From Figure 3.12, it can be observed what happens with the implementation of only the phase-shifted control. Initially, there is a reduction in current ripple. However, following a fault in one converter, the cancellation of harmonic content is lost. Based on these considerations, it was chosen to adopt a fault-tolerant control of the phase shift adjustment type. The calculations are as follows:

$$\frac{2 \cdot \pi}{N_a + N_r - N_f} = \frac{2 \cdot \pi}{3 + 0 - 1} = \pi \tag{3.2}$$

Therefore, the carriers need to be phased by 180 degrees. Since the first carrier is at zero degrees, the second carrier was changed from 240 degrees to 180 degrees. Upon implementing this fault-tolerant control within the system, the graphs depicted in figure 3.13 are obtained.

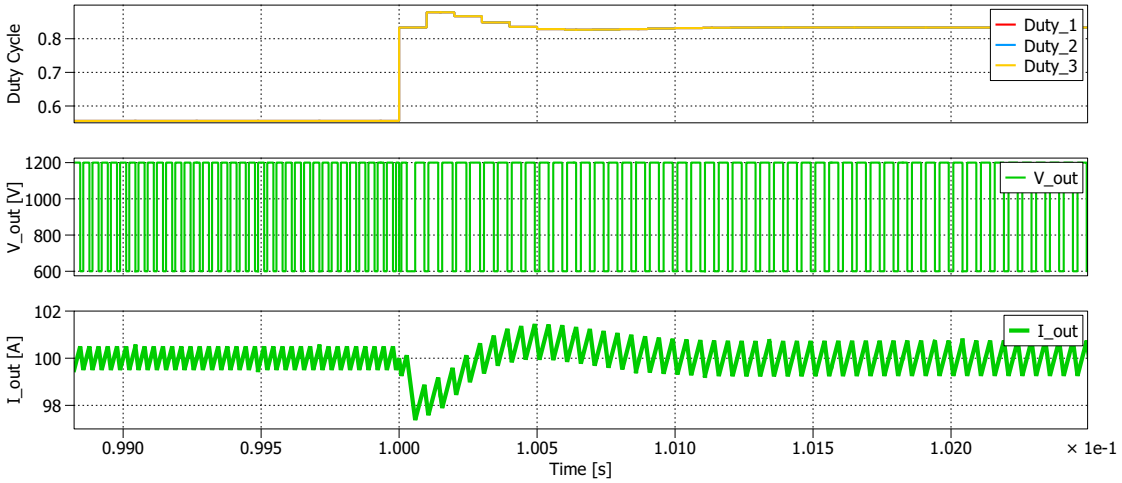

Figure 3.13: Output values with fault tolerant control.

As you can see, harmonic cancellation has been achieved, thus maintaining the required performance.

3.2.4 Ideal charge mode

As a second simulation, the charging mode scenario was chosen. In this case, the system setup remains the same as in the previous scenario. The system configuration is illustrated in figure 3.14

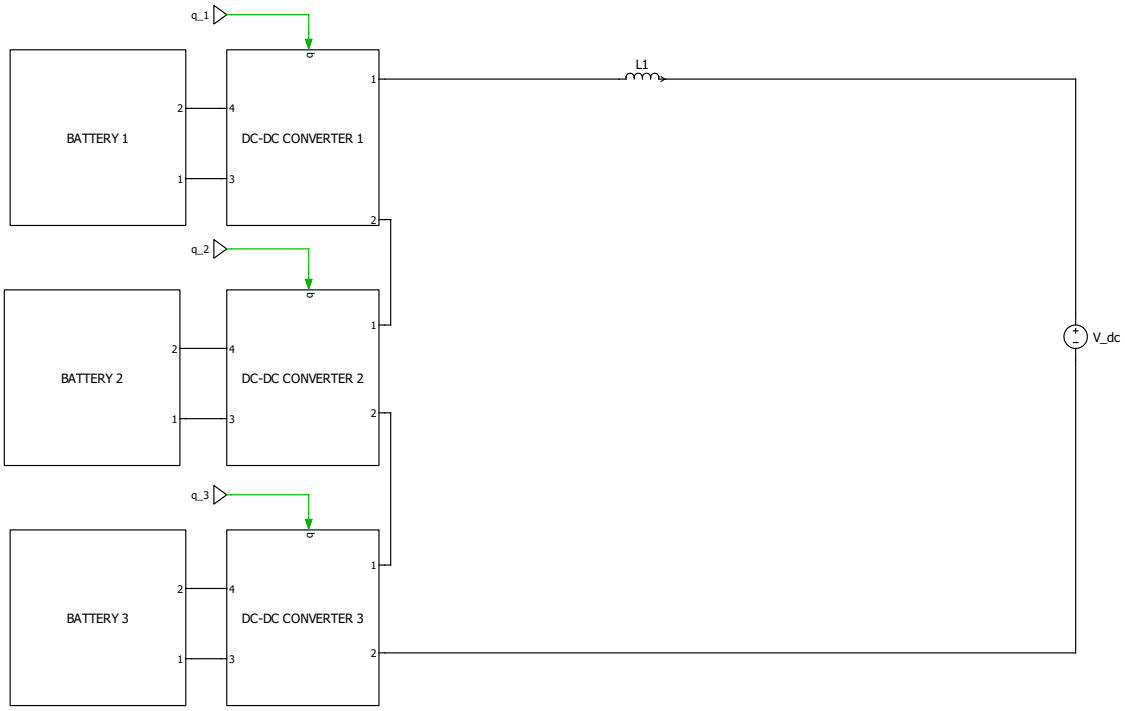

Figure 3.14: Ideal system for charge mode.

Following a fault occurrence in one of the converters, particularly in the case of an open-circuit fault, control over the converter is lost. As a result, current will flow through the diode in anti-parallel with the high-side switch. This leads uncontrolled charging of the battery pack, even when it is fully charged, ultimately resulting in component damage. To prevent damage to the component, the implementation of bypass and phase shift has been chosen to maintain harmonic performance in the healthy modules, as depicted in Figure 3.15.

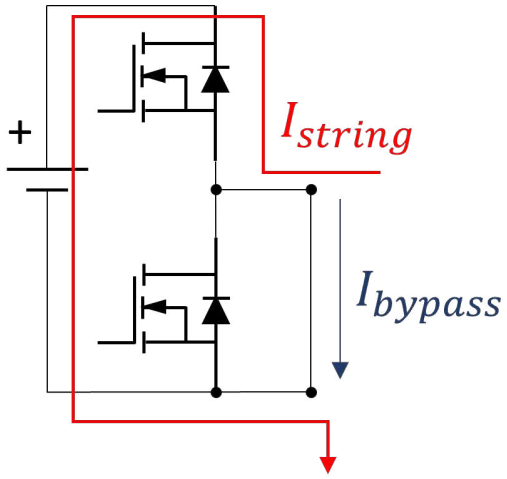

Figure 3.15: Bypass for charge mode.

Through this implementation, we not only prevent damage to a component (the battery pack), but we also enable battery recharging while maintaining harmonic performance. The results of the fault-tolerant control implementation are depicted in Figure 3.16.

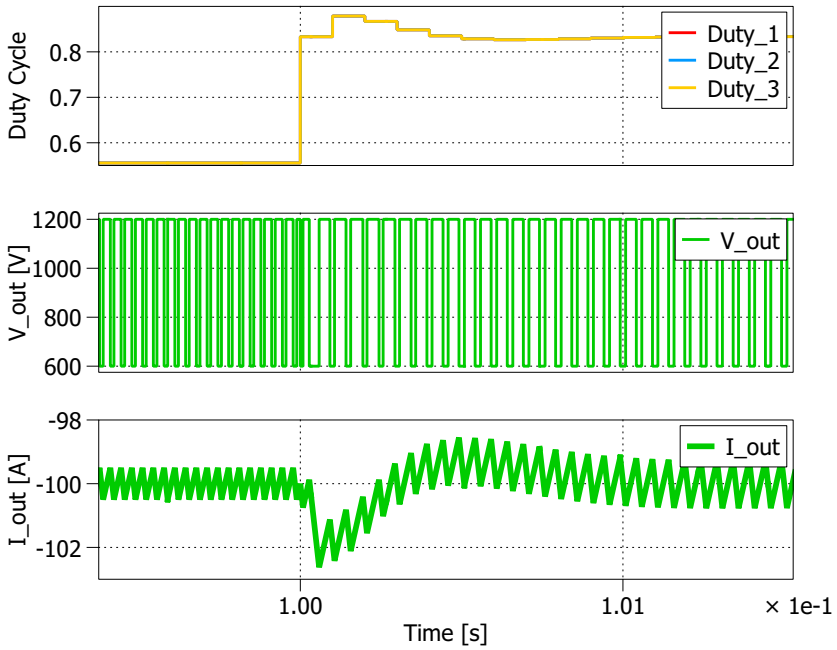

Figure 3.16: Output values with fault tolerant control in charge mode.

3.2.5 Ideal Parallel string

As the final case under consideration, we have examined the scenario of a string fault. The system consists of 9 modules, as depicted in figure 3.17. In this configuration, each module is connected in series with two other modules.

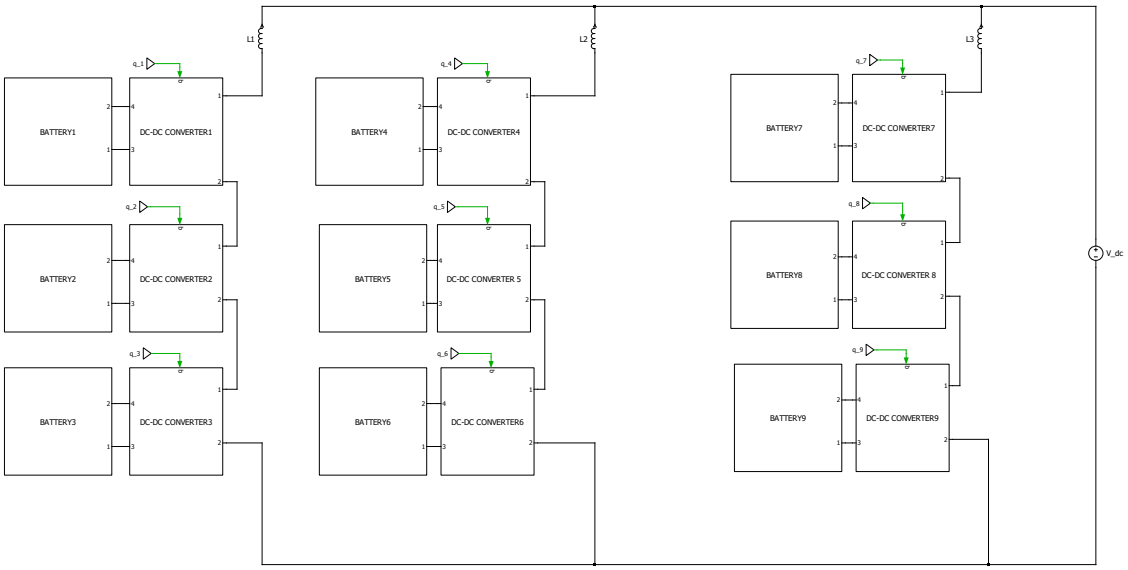

Figure 3.17: Ideal system for parallel string.

Assuming a fault occurs on each module within a string, the system will consist of two healthy strings in parallel, with the diodes in antiparallel of the faulty modules creating a short circuit with the healthy modules as shown in Figure 3.18. To address this issue, the contactors in the string where the fault occurred are opened.

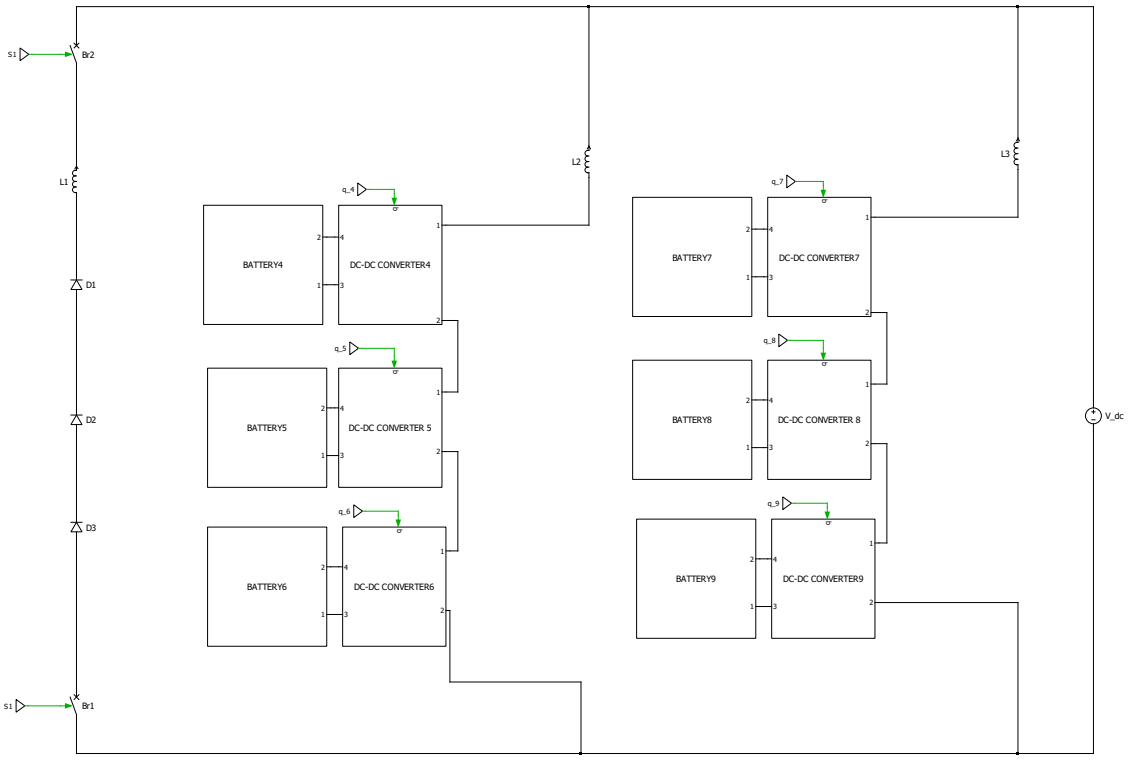

Figure 3.18: Fault on parallel strings.

Simulation results suggest that there is no significant difference in terms of harmonic content, as the phase shift occurs between the modules within the string rather than between the strings. What we can observe is that since the strings are in parallel, the current will flow equally through the other two.

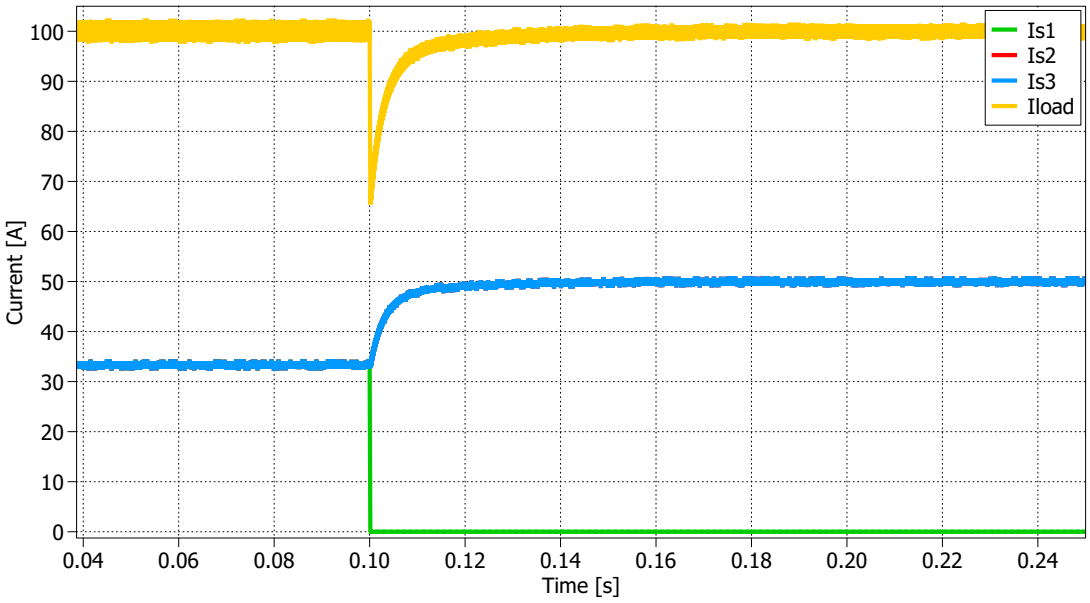

Figure 3.19: Currents of parallel strings.

Chapter 4

Simulation validation

This chapter will examine three real-life cases of fault tolerant control of modular multilevel shipboard storage system, with a specific focus on:

- Discharge modes
- Charging modes
- Parallel string configuration

4.1 Discharging mode

For the first simulation, the focus will be on the discharge mode with digital control. The system consists of three battery packs, each equipped with its own converter. An inductor has been incorporated between the converters and the resistive load to filter the current. Additionally, a capacitor has been added in parallel to the load to maintain a constant output voltage. The resistive load is chosen to emulate the typical behavior of a ship. The system is illustrated in the figure 4.1

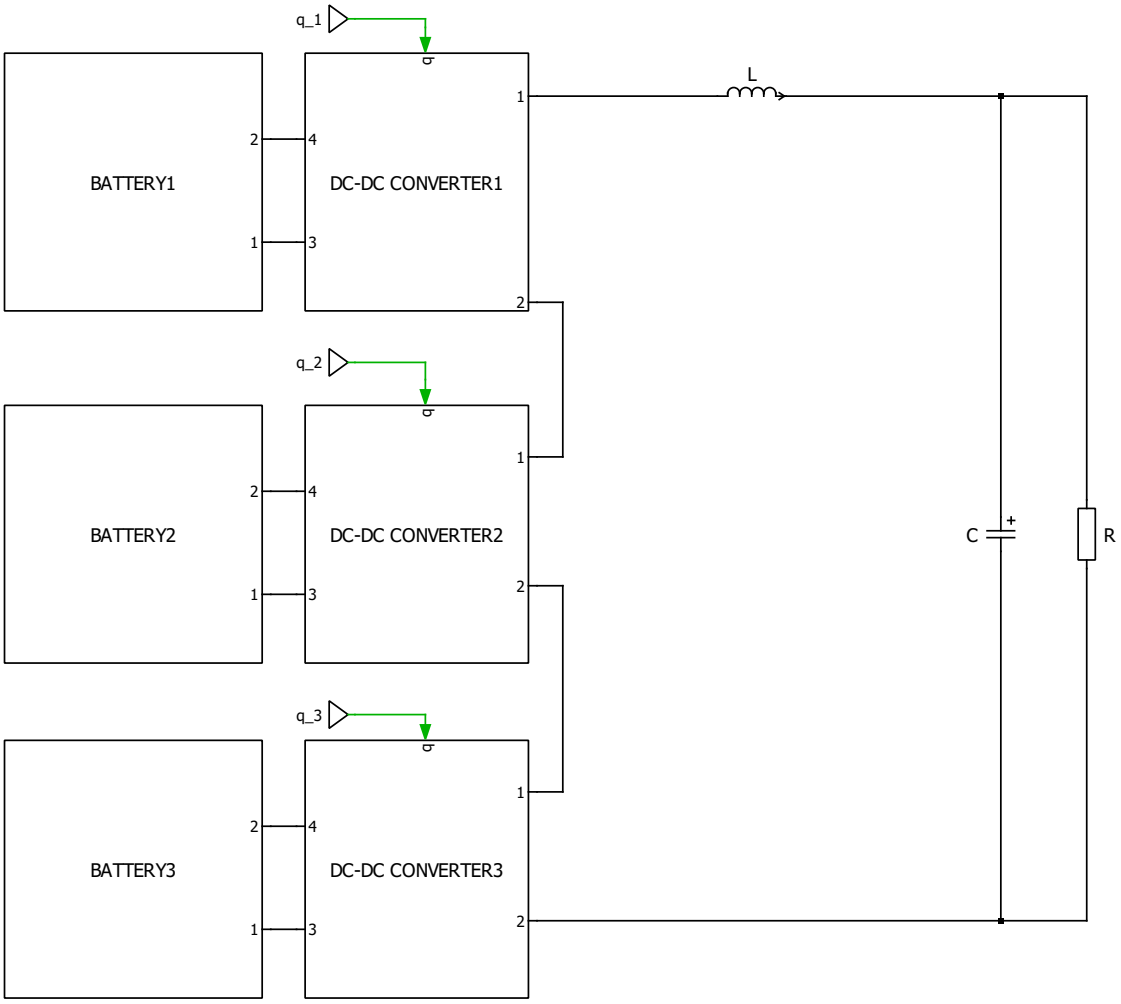

Figure 4.1: Circuit for discharge mode.

4.1.1 Simulation results for discharge mode

In this subsection, the results obtained from simulating a fault tolerant control in a converter due to its discharge mode will be presented. The initial parameters used during the simulation are listed in Table 4.1.

Simulation Parameters	
V_{out}	1000 V
V_{cell}	3.6 V
V_{batt}	600 V
$Number\ of\ Module$	3
n_s	167
n_p	0.0025
L	4.44 mH
C	1 mF
R	10 Ω
f_{sw}	10 kHz
ω_i	$800 \cdot 2 \cdot \pi\ rad/s$
$K_{p,i}$	$w_{b,i} \cdot L$
$K_{i,i}$	$0.2 \cdot w_{b,i} \cdot K_p$
$K_{p,v}$	$w_{b,v} \cdot C$
$K_{i,v}$	$0.1 \cdot w_{b,v} \cdot K_{p,v}$
SOC_1	100 %
SOC_2	95 %
SOC_3	90 %

Table 4.1: Simulation parameters for discharge mode.

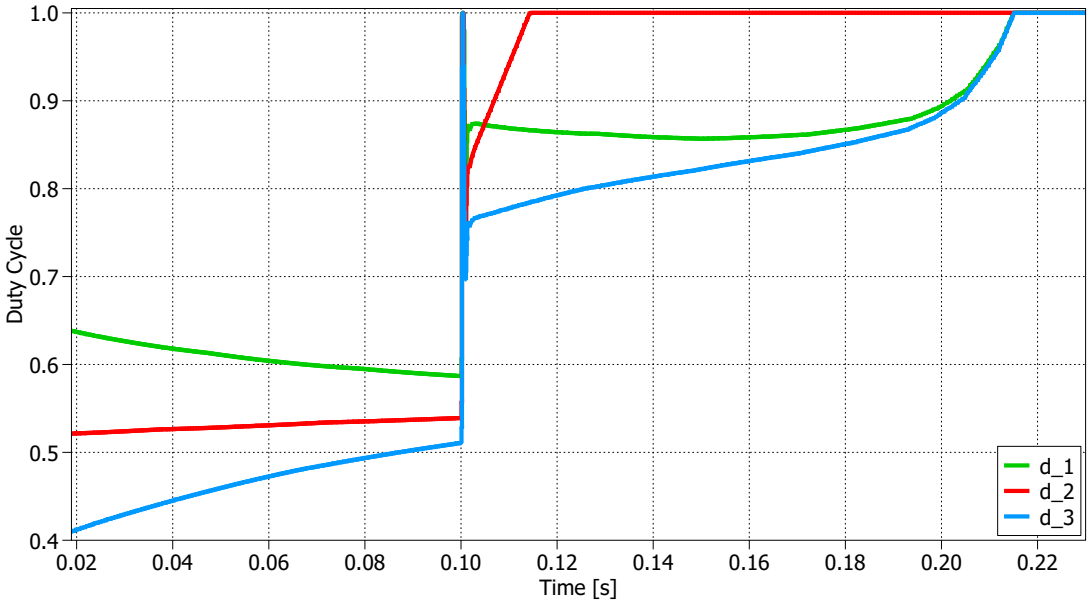

Figure 4.2: Duty cycle in discharging mode.

The first graph depicted in Figure 4.2 illustrates the time evolution of the duty cycle for the three modules. As observed, the initial duty cycles are not identical, due to the fact that the three battery packs start from different initial state-of-charge. At time instant t=0.1 seconds, a fault occurs in Converter 2, which is bypassed. Regarding the other two modules, in response to the fault, they adjust their duty cycles to ensure continuity of service while maintaining the same performance. Since, at the same moment, the batteries are discharging, the duty cycles do not remain constant until reaching their maximum values.

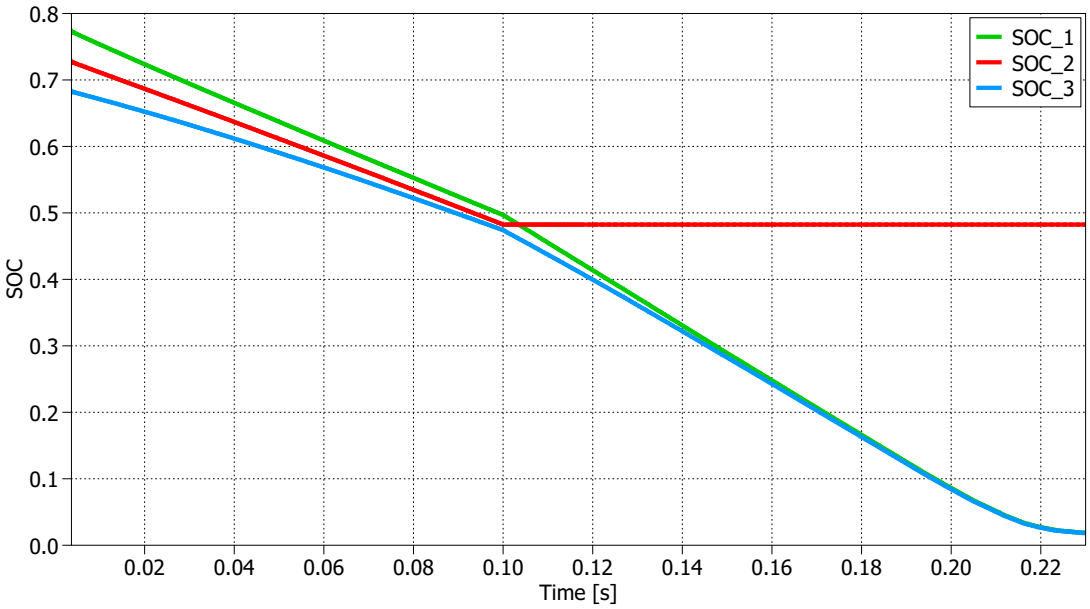

Figure 4.3: SOC in discharging mode.

The graph in Figure 4.3 depicts the time evolution of the state of charge (SOC) for the three modules. As observed, the slopes of the state of charge are nearly identical among them before the fault. After the fault, the state of charge of Module 2 remains constant over time, while the state of charge of the other two modules undergo changes in their slopes. This indicates that the modules are discharging at a much faster rate to maintain the performance required by the system.

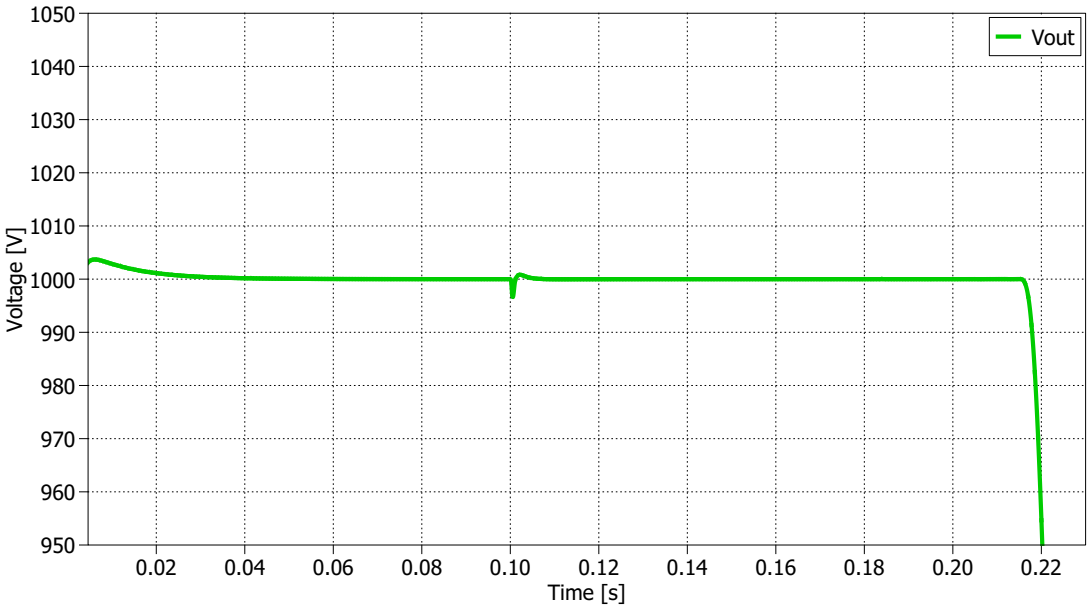

Figure 4.4: Output voltage in discharging mode.

As the final graph of this simulation, Figure 4.4 illustrates the time evolution of the voltage across the resistive load. It is noticeable that at the moment of the fault occurrence, there is a voltage dip, but this lasts for only a few instants, as the voltage quickly returns to its initial conditions due to the voltage control implementation. Towards the end of the simulation, the voltage decreases as the batteries are nearly depleted, unable to deliver the performance required by the system.

4.2 Charging mode

For the second simulation, the focus will be on the charge mode with digital control. The system consist of three battery packs, each equipped with its own converter. An inductor has been incorporated between the converters and the voltage source. The voltage source is chosen to emulate the typical behavior of a ship during the charging mode. The system is illustrated in the figure 4.5

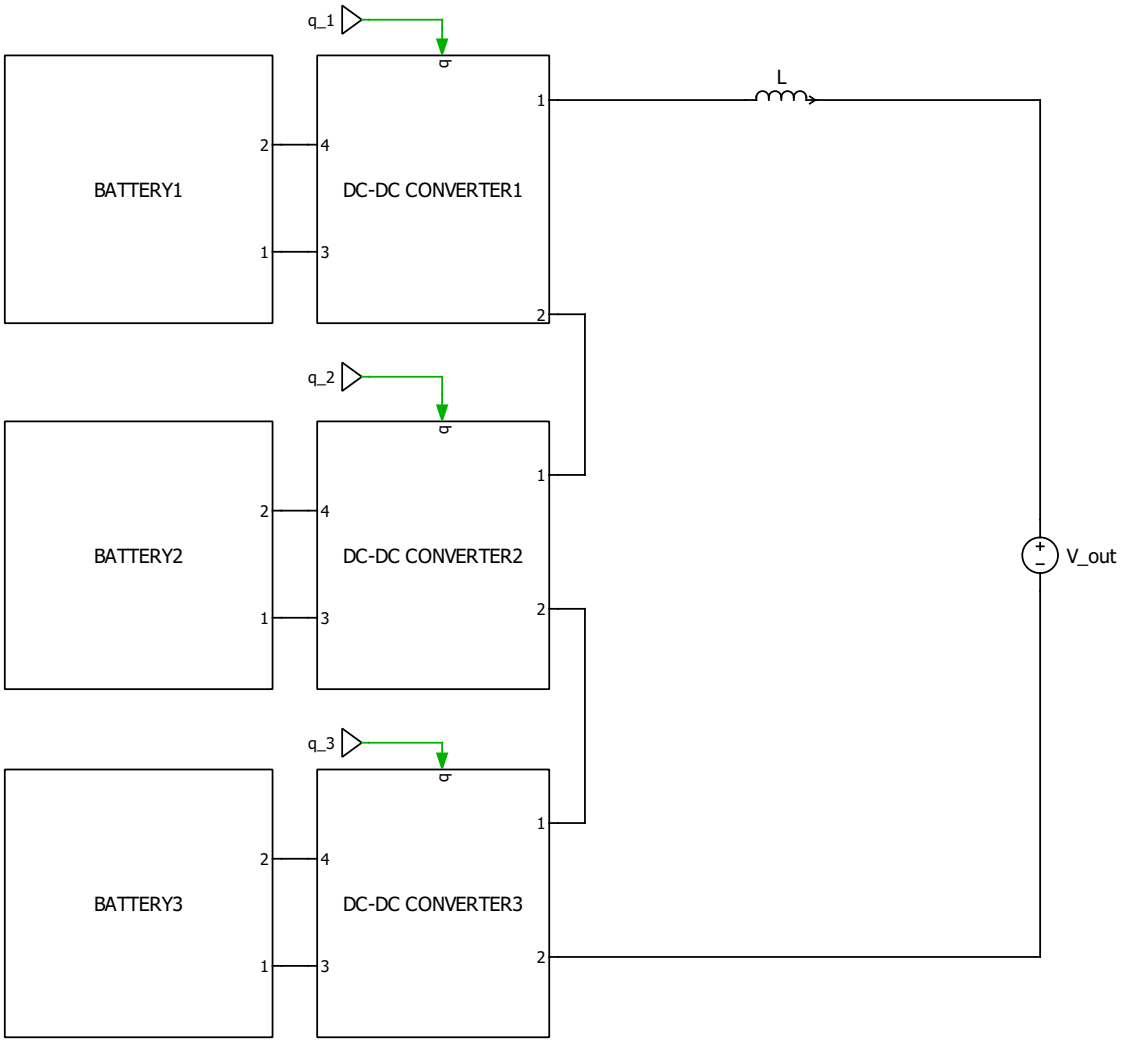

Figure 4.5: Circuit for charge mode.

4.2.1 Simulation results for charging mode

In this subsection, the results obtained from simulating a fault tolerant control in a converter during its charging will be presented. Before delving into the discussion of these results, the initial parameters used during the simulation will be detailed. The initial parameters are listed in Table 4.2.

Simulation Parameters	
V_{source}	1000 V
V_{cell}	3.6 V
V_{batt}	600 V
$Number\ of\ Module$	3
n_s	167
n_p	0.01
L	4.44 mH
f_{sw}	10 kHz
ω_i	$800 \cdot 2 \cdot \pi\ rad/s$
$K_{p,i}$	$w_{b,i} \cdot L$
$K_{i,i}$	$0.2 \cdot w_{b,i} \cdot K_p$
SOC_1	90 %
SOC_2	87 %
SOC_3	85 %

Table 4.2: Parameters for charge mode simulation.

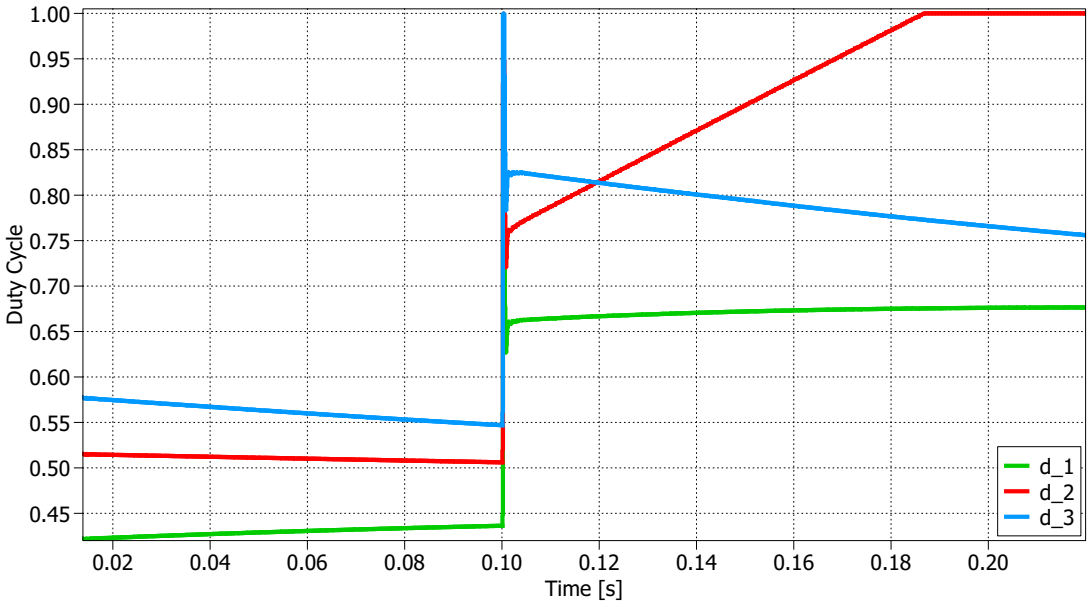

Figure 4.6: Duty cycle in charging mode.

Figure 4.6 depicts the time evolution of the duty cycle. As in the previous case, they start with different initial conditions due to varying state of charge values. Following the

fault occurrence in Module 2, it is bypassed to ensure system continuity

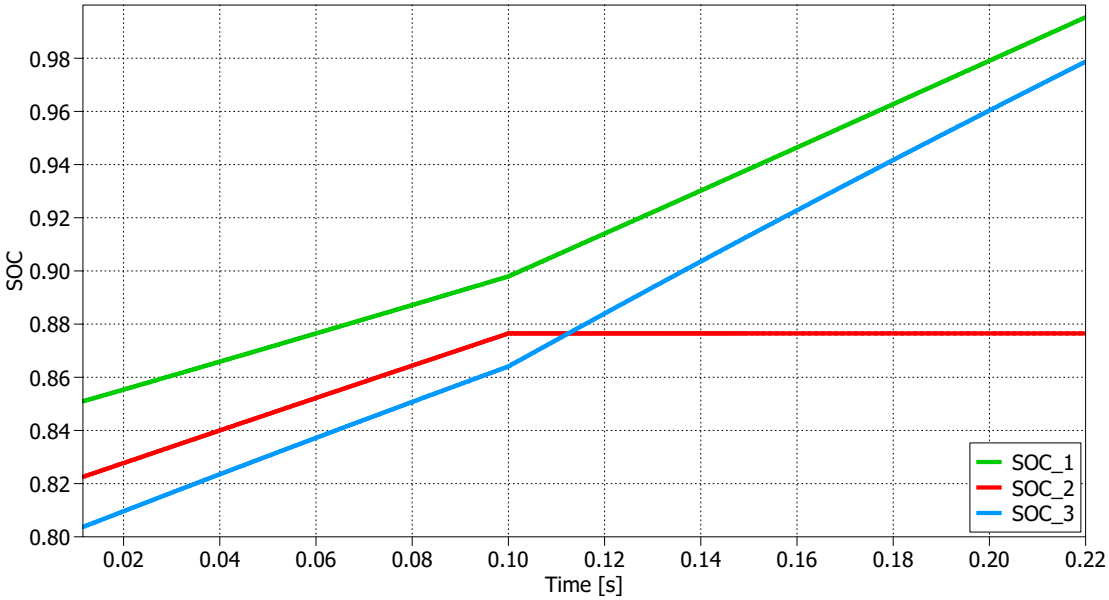

Figure 4.7: SOC in charging mode.

Figure 4.7 illustrates the time evolution of the state of charge (SOC) for the three modules. Before the fault occurrence, the SOC exhibits an identical increasing trend for all three modules, indicating the charging phase. Following the fault in Module 2, its SOC remains constant as it is bypassed. In contrast, the SOC of the other two modules increases at a steeper rate due to the higher current supplied, resulting in a faster charging process.

4.3 Parallel string

For the final simulation, the primary focus is on the parallel string with digital control. The system consists of three parallel strings, each comprising three battery packs, each equipped with its individual converter. An inductor has been incorporated into each string, serving as a filter. At the system's output, a resistive load is connected to replicate

the ship's load. The overall system configuration is visually represented in Figure 4.8.

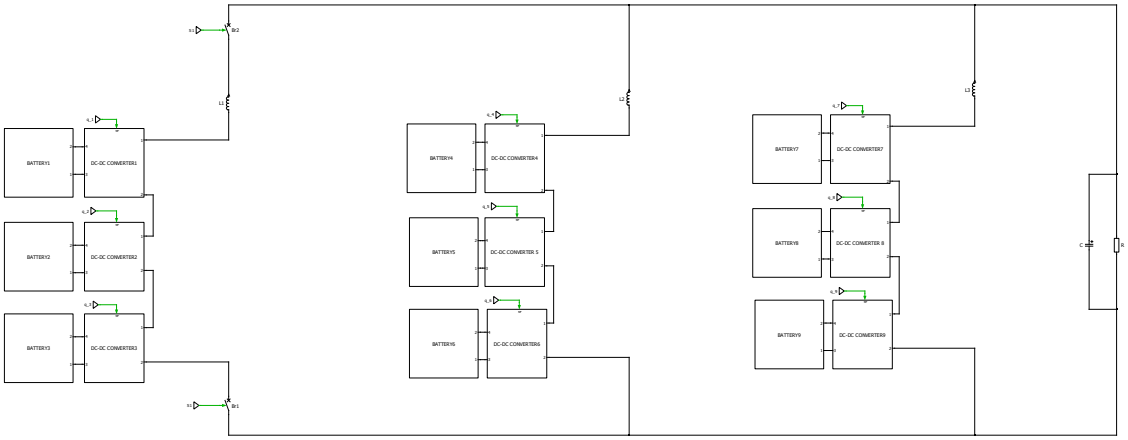

Figure 4.8: Parallel String.

4.3.1 Simulation results for parallel string

In this subsection, the results obtained from simulating a fault tolerant control in a parallel string will be presented. Before delving into the discussion of these results, the initial parameters used during the simulation will be detailed. The initial parameters are listed in Table 4.3.

Simulation Parameters	
V_{out}	1000 V
V_{cell}	3.6 V
V_{batt}	600 V
$Number\ of\ Module$	9
n_s	167
n_p	0.01
L	4.44 mH
C	1 mF
R	10 Ω
f_{sw}	10 kHz
ω_i	$500 \cdot 2\pi\ rad/s$
$K_{p,i}$	$w_b \cdot L$
$K_{i,i}$	$0.2 \cdot w_b \cdot K_p$
$K_{p,v}$	$w_b \cdot L$
$K_{i,v}$	$0.1 \cdot w_b \cdot K_p$
SOC_1	100 %
SOC_2	98 %
SOC_3	95 %
SOC_4	100 %
SOC_5	98 %
SOC_6	95 %
SOC_7	100 %
SOC_8	98 %
SOC_9	95 %

Table 4.3: Parameters for parallel string mode Simulation.

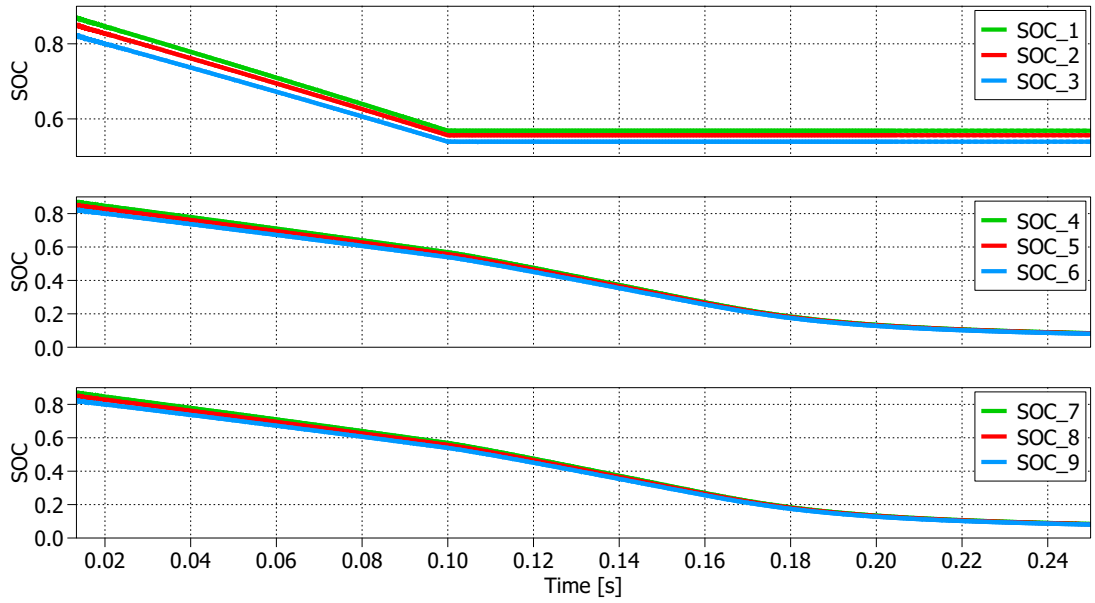

Figure 4.9: SOC in Parallel String.

In Figure 4.9, the SOC variation of all modules divided by each string are depicted. As observed, the behavior before the fault is identical across all strings. Following the fault occurrence in the first string, the system responds by disconnecting the affected string. Regarding the other two strings, the state of charge trends will change, exhibiting a increase in slope as they need to supply more energy. However, the trends remain identical across the two unaffected strings.

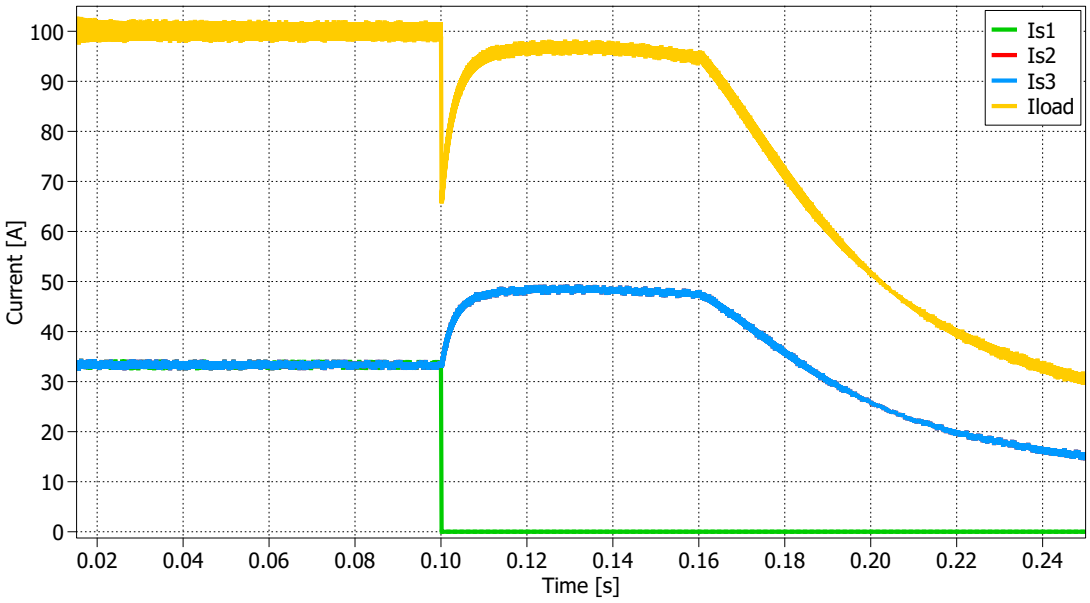

Figure 4.10: Current in Parallel String.

In Figure 4.10, the temporal behavior of the current in the load and the current profiles in the three strings is depicted. Initially, the current profiles in the three strings are identical, as the strings are uniform, resulting in overlapping currents. Following the occurrence of a fault, the affected string is disconnected, leading to zero current in that string. The unaffected strings must then provide additional current to compensate for the loss of one string. However, this occurs only up to a certain point, as the batteries are nearly depleted.

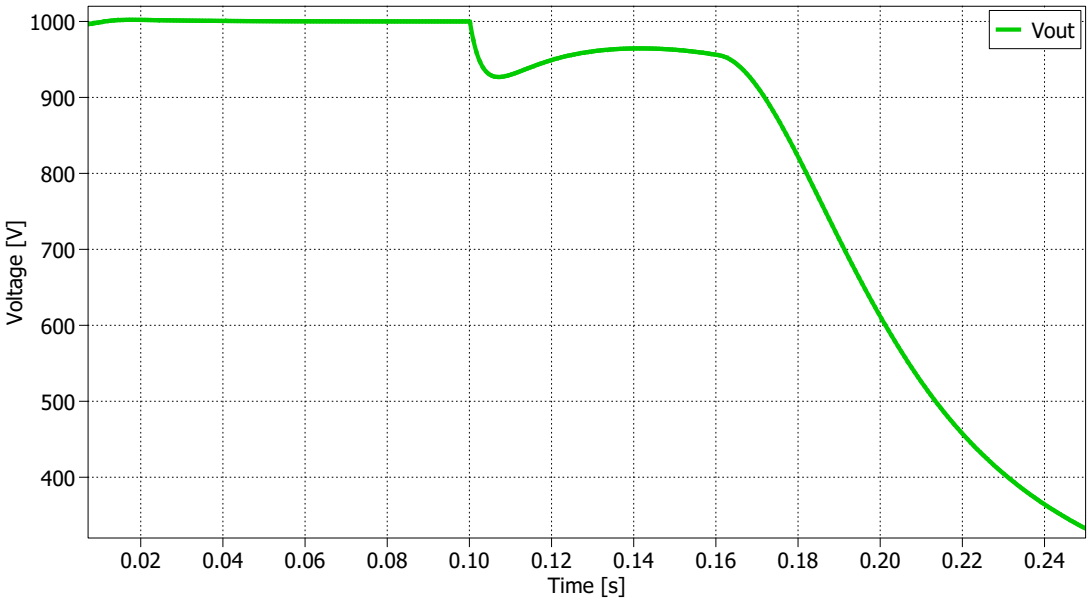

Figure 4.11: Voltage in Parallel String.

In the last figure, 4.11, the temporal variation of the voltage across the load is illustrated. Before to the fault occurrence, this voltage remains constant, thanks to the implemented voltage control. At the moment of the fault, the system experiences a loss and attempts to return to the pre-fault conditions. However, it is unable to do so, as the other two strings lack sufficient energy to restore the system to its initial state.

Chapter 5

Conclusions

This thesis investigates the implementation of a modular structure comprising a set of modules, each equipped with a battery pack and its corresponding converter, intended for deployment in naval applications. The primary objective is to reduce emissions and progress towards complete electrification of the maritime sector. Concurrently, various fault-tolerant control systems have been developed and tested for the converters. The simulation results yield several significant insights:

- Regarding discharge mode, the system demonstrates prompt dynamic response to faults by efficiently distributing the energy required by the load among the intact modules. This ensures the maintenance of required performance metrics, such as output voltage and minimal current ripple, until the batteries are nearly depleted.
- In charging mode, following a fault in one module, the system reacts by bypassing the affected module to ensure operational continuity. Meanwhile, the other modules increase their charging rate to compensate for the additional current demand. This dynamic system adaptation enables the maintenance of desired performance levels and ensures the integrity of the faulty module.

- In the parallel string configuration, pre-fault behavior shows uniform state-of-charge (SOC) across all strings. However, after a fault occurs in one string, the system responds by disconnecting the affected string and redistributing the load among the remaining strings. This ensures uninterrupted system operation, even as the batteries approach depletion.

Given the criticality of safety in naval applications, it is recommended to oversize the battery packs to account for the loss of a module, thereby ensuring operational continuity and the safety of the vessel and its crew.

5.1 Personal Contribution

My personal contributions to this thesis can be summarized as follows.

- Conducting a comprehensive literature review on fault-tolerant strategies and ship architecture to establish a solid theoretical foundation.
- Investigating switch faults and their implications on system performance and reliability.
- Analyzing the impact of different module configurations on system output and efficiency.
- Undertaking the task of sizing battery packs to ensure optimal performance and longevity
- Examining various fault-tolerant control strategies specific to Modular Multilevel Converters (MMCs) to mitigate risks and enhance system resilience.

- Developing and implementing fault-tolerant control algorithms in the C programming language tailored for discharge mode operations.
- Designing and implementing fault-tolerant control algorithms in C language optimized for charge mode operations.
- Developing and implementing fault-tolerant control algorithms in C language suitable for parallel string configurations.

Ringraziamenti

Ringrazio di cuore tutti coloro che hanno contribuito al mio percorso di studi e alla realizzazione di questo progetto.
Desidero esprimere un profondo ringraziamento al mio relatore, il Professor Michele Angelo Pastorelli, e al mio co-relatore Fabio Mandrile per la loro costante disponibilità e tempestività nel supportarmi e nell'offrirmi preziosi consigli lungo il cammino accademico.
Desidero esprimere profondo riconoscimento ai miei genitori per avermi offerto l'opportunità di proseguire gli studi a Torino. Inoltre, vorrei estendere il mio ringraziamento a tutti i miei familiari, che mi hanno sostenuto in ogni fase del mio percorso universitario. Il loro supporto e incoraggiamento sono stati fondamentali per il mio successo accademico.
Non posso dimenticare di ringraziare anche i miei stimati colleghi ed amici, che con la loro collaborazione e sostegno reciproco hanno reso più stimolante e gratificante l'esperienza universitaria, arricchendola di valore e crescita personale.
Vorrei inoltre esprimere un particolare ringraziamento ai miei amati cani Leone e Sansa, che hanno reso i momenti di studio più piacevoli e hanno riempito la mia vita di gioia, conforto e amore incondizionato. La loro presenza affettuosa ha reso ogni istante della mia vita quotidiana speciale e significativo.

Bibliography

[1] Luona Xu et al. «A Review of DC Shipboard Microgrids—Part I: Power Architectures, Energy Storage, and Power Converters». In: *IEEE Transactions on Power Electronics* 37.5 (2022), pp. 5155–5172.

[2] Qian Xiao et al. «Review of fault diagnosis and fault-tolerant control methods of the modular multilevel converter under submodule failure». In: *IEEE Transactions on Power Electronics* (2023).

[3] Simone Mongelli. «Management of a Modular Battery System for Shipboard Application». Politecnico di Torino, 2022.

[4] Geddam Kiran Kumar and Devaraj Elangovan. «Review on fault-diagnosis and fault-tolerance for DC–DC converters». In: *IET Power Electronics* 13.1 (2020), pp. 1–13.

[5] Binbin Li et al. «Fault-tolerant control of medium-voltage modular multilevel converters with minimum performance degradation under submodule failures». In: *IEEE Access* 6 (2018), pp. 11772–11781.

[6] Iustin Radu Bojoi and Eric Armando. *Dispense corso di Fondamenti di Azionamenti Elettrici*. Materiale didattico. Anno accademico 2020/2021.

[7] Iustin Radu Bojoi. *Power Electronics for e-Mobility*. Materiale didattico. Anno accademico 2022/2023.